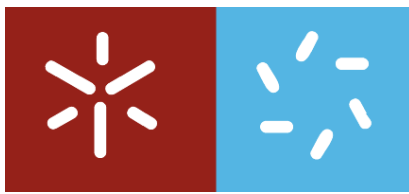


Universidade do Minho
Escola de Ciências

Flávia Natacha Silva Sousa

**Cell death mechanisms and targets of new
fluorescent dyes with antiproliferative
activity**



Universidade do Minho
Escola de Ciências

Flávia Natacha Silva Sousa

**Cell death mechanisms and targets of new
fluorescent dyes with antiproliferative
activity**

Tese de Mestrado
Mestrado em Genética Molecular

Trabalho realizado sob a orientação de
**Professora Doutora Maria João Marques
Ferreira Sousa Moreira**
**Professora Doutora Maria Sameiro Torres
Gonçalves**

Fevereiro de 2018

Declaração

Nome: Flávia Natacha Silva Sousa

Endereço Eletrónico: sousa.s.flavia@gmail.com

Telefone: 917182680

Nº Cartão Cidadão: 13278792

Título da Tese de Mestrado:

Cell death mechanisms and targets of new fluorescent dyes with antiproliferative activity

Orientadores:

Professora Doutora Maria João Marques Ferreira Sousa Moreira

Professora Doutora Maria Sameiro Torres Gonçalves

Instituição de Acolhimento:

Centro de Biologia Molecular e Ambiental (CBMA)

Ano de conclusão: 2018

Designação do Mestrado:

Mestrado em Genética Molecular

DE ACORDO COM A LEGISLAÇÃO EM VIGOR, NÃO É PERMITIDA A REPRODUÇÃO DE
QUALQUER PARTE DESTA TESE

Universidade do Minho, 28 de Fevereiro de 2018

Assinatura: _____

Agradecimentos

A elaboração deste trabalho não seria possível sem o apoio e a colaboração de todas as pessoas que contribuíram de forma direta ou indireta ao longo deste mestrado, desta forma gostaria de deixar algumas palavras, e um profundo sentimento de agradecimento.

Às minhas orientadoras, Doutora Maria João Sousa e Doutora Maria Sameiro Gonçalves, o meu profundo agradecimento pela orientação, pelo apoio incondicional e profissionalismo que permitiu a conclusão deste trabalho e também pela oportunidade e privilégio de concretização do mesmo, que tanto contribuiu para o enriquecimento da minha formação académica e científica. O meu sincero obrigado às duas.

À Doutora Manuela Côrte-Real e Doutora Susana Chaves, agradeço a simpatia e total disponibilidade, assim como todas ideias e ajuda prestada durante esta etapa.

A todos os meus colegas da Micro I, à Cátia, à Joana Guedes, à Anabela, ao João, ao António, à Rita, à Leslie, ao Vítor e à Joana agradeço todos bons momentos passados no laboratório, a partilha de conhecimentos, o companheirismo, a força, a paciência e a coragem. Agradeço também aos restantes colegas dos outros laboratórios que tive a oportunidade de conhecer, obrigada por tudo, juntos formamos uma grande e bela família.

A todos os técnicos e funcionários do departamento de biologia, que tornaram e tornam o departamento um local único para trabalhar, em especial ao Senhor Luís por ser o melhor “vizinho da frente” que um investigador pode ter, e à Núria por toda a disponibilidade e ajuda prestada.

Aos meus amigos, em especial à Cris, à Ju, à Daniela, à Ângela e à Carlinha agradeço a amizade, o apoio incondicional e a qualquer hora do dia, a motivação que sempre me deram e que me ajudou a ultrapassar mais esta etapa.

Por fim, à minha família, em especial aos meus pais, ao meu irmão, avó e namorado, um enorme obrigado por acreditarem e nunca desistirem de mim, pelas palavras doces e pela transmissão de confiança e força. Sem vocês não teria conseguido. A minha enorme gratidão.

Abstract

Cell death mechanisms and targets of new fluorescent dyes with antiproliferative activity

Phenoxazine derivatives have been the subject of an increasing research in life sciences due to their antiproliferative properties with potential applications as antitumor and antimicrobial agents, leading to the design and synthesis of novel active compounds suitable for human use.

Previous studies in our laboratory have shown that a newly synthesized phenoxazine derivative (MSG-111-cd3) induces yeast cell death through a regulated process which may be mediated by the permeabilization of the vacuolar membrane, without the involvement of autophagy and mitochondrial pathways. The interesting potential of this newly phenoxazine compound lead us to study a compound of the same family (C9) that differ from MSG-111-cd3 only in a single substitution of its extended aromatic system which considerably increases its antifungal activity.

The yeast *Saccharomyces cerevisiae* represents a unique eukaryotic model used in drug-discovery process due to the high conservation of basic cellular processes present in higher organisms.

In the present work, we aimed to characterize the intracellular distribution and the cell death mechanism underlying C9 activity using the yeast *Saccharomyces cerevisiae* as a model. The results showed that C9 compound accumulates in the vacuolar membrane and the perinuclear endoplasmic reticulum. We observed that Pep4p and Yca1p play a protective and effector role, respectively, in mediation of C9-induced cell death. Although Atg5p displayed a protective role, autophagy does not seem be involved. As a whole, the results point to the occurrence of a regulated cell death process mediated by the vacuolar permeabilization and mitochondrial involvement.

This work provides new insights in the use of phenoxazine derivatives as antifungal agents, characterizing their activity in order to evaluate their potential application.

Resumo

Mecanismos de morte e alvos de novos compostos fluorescentes com atividade antiproliferativa

Os derivados de fenoxazina têm sido objeto de crescente investigação nas ciências da vida devido às suas propriedades antiproliferativas e potencial aplicação como agentes antitumorais e antimicrobianos, levando ao design e síntese de novos compostos ativos com baixa toxicidade, adequados para uso humano.

Estudos preliminares no nosso laboratório demonstraram que um derivado de fenoxazina recentemente sintetizado (MSG-111-cd3) induz morte celular em leveduras através de um processo regulado que parece ser mediado pela permeabilização da membrana vacuolar, sem o envolvimento da autofagia e da via mitocondrial. O interessante potencial deste novo composto de fenoxazina levou-nos a estudar outro composto desta família (C9) que difere do MSG-111-cd3 apenas numa única substituição do seu sistema aromático, o que aumenta consideravelmente a sua atividade antifúngica.

A levedura *Saccharomyces cerevisiae* representa um modelo eucariótico único, que pode ser usado no processo de descoberta de novas drogas devido à elevada conservação dos processos celulares básicos presentes em organismos superiores.

O objetivo do presente trabalho consistiu em caracterizar a distribuição intracelular e o mecanismo de morte celular subjacente à atividade do C9, utilizando a levedura *Saccharomyces cerevisiae* como modelo biológico. Os resultados demonstraram que o composto C9 acumula-se tanto na membrana vacuolar como na membrana perinuclear do retículo endoplasmático. Observamos também que as proteínas Pep4p e a Yca1p exibem um papel protetor e efetor, respectivamente, na mediação da morte celular induzida pelo C9. Embora a proteína Atg5p tenha um papel protetor da morte induzida por este composto, a autofagia não parece estar envolvida. Em conjunto, os resultados apontam para a ocorrência de um processo de morte celular regulado, mediado pela permeabilização vacuolar e o envolvimento mitocondrial.

Este trabalho fornece novo conhecimento sobre o uso de derivados de fenoxazina como agentes antifúngicos, caracterizando sua atividade de forma a avaliar o seu potencial de aplicação.

Table of contents

Declaração.....	ii
Agradecimentos	iii
Abstract	v
Resumo	vii
Table of contents.....	ix
List of abbreviations and acronyms.....	xi
List of figures	xiii
List of tables	xiv
Chapter I	
I. Introduction	3
I.1 Cell death	3
I.1.1 Cell death induced by lysosomal membrane permeabilization	6
I.2 Yeast cell death	9
I.3 Phenoxazine and benzophenoxazine derivatives	12
Chapter II	
II. Aims	19
Chapter III	
III. Material and Methods	23
III.1 Yeast strains	23
III.2 Media and growth conditions.....	23
III.3 C9 stock solution preparation and treatment.....	25
III.4 Production of BY 4741 rho ⁰ strain.....	25
III.5 Cell viability assays and proteins synthesis inhibition.....	25
III.6 Assessment of C9 intracellular distribution	26
III.7 Assessment of plasma membrane integrity.....	26
III.8 Assessment of vacuole membrane permeabilization	26
III.9 Assessment of mitochondrial network fragmentation	26
III.10 Assessment of the accumulation of reactive oxygen species	27

III.11	Cell cycle analysis	27
III.12	Assessment of autophagy induction	27
III.12.1	GFP-Atg8 protein localization	28
III.12.2	Western blot analysis	28
III.13	Epifluorescence microscopy and flow cytometry	29
III.14	Statistical Analysis.....	29
 Chapter IV		
IV.	Results	33
IV.1	Intracellular distribution of C9 compound.....	33
IV.2	C9 treatment induces loss of cell viability in the yeast <i>Saccharomyces cerevisiae</i>	33
IV.3	Vacuolar involvement in cell death induced by C9.....	34
IV.4	Mitochondrial involvement in cell death induced by C9	37
IV.5	Metacaspase involvement in cell death induced by C9.....	40
IV.6	Assessment of the accumulation of reactive oxygen species.....	40
IV.6	Autophagy involvement in cell death induced by C9	41
IV.7	Assessment of nuclear changes induced by C9 treatment.....	45
IV.8	Assessment of plasma membrane integrity	46
 Chapter V		
V.	Discussion and Future perspectives	51
 Chapter VI		
VI.	References.....	59
 Chapter VII		
VII.	Supplementary data	69

List of abbreviations and acronyms

AIF	Apoptosis Inducing Factor
ANOVA	Analysis of Variance
ATP	Adenosine Triphosphate
CFU	Colony Forming Units
CHX	Cyclohexadienyl
DAPI	4',6- diamidino-2-phenylindole
DIC	Differential Interferential Contrast
DHE	Dihydroethidium
DMSO	Dimethyl Sulfoxide
EtOH	Ethanol
ER	Endoplasmic Reticulum
GFP	Green Fluorescent Protein
HRP	Horseradish Peroxidase
H₂O₂	Hydrogen Peroxide
LAMP	Lysosomal-associated Membrane Protein
LMP	Lysosomal Membrane Permeabilization
MIC	Minimum Inhibitory Concentration
MMP	Mitochondrial Membrane Permeabilization
MOMP	Mitochondrial Outer Membrane Permeabilization
OD	Optical Density
PBS	Phosphate Buffer Saline
PI	Propidium Iodide
PCD	Programmed Cell Death
PCR	Polymerase Chain Reaction
PTP	Permeability Transition Pore
PVDA	Polyvinylidene Fluoride
RCD	Regulated Cell Death
ROS	Reactive Oxygen Species
RP	Rapamycin
rpm	rotations per minute

SD	Standard Deviation
SDS-PAGE	Sodium Dodecyl Sulphate-Polyacrylamide Gel Electrophoresis
TCA	Trichloroacetic Acid
TNF	Tumor Necrosis Factor
TUNEL	Terminal deoxynucleotidyl transferase dUTP nick end Labeling
VMP	Vacuolar Membrane Permeabilization
YEPD	Yeast Extract Peptone Dextrose
YEPDA	Yeast Extract Peptone Dextrose Agar
YEPGA	Yeast Extract Peptone Glycerol Agar

List of figures

Figure I.1 - Representation of apoptosis intrinsic pathway	4
Figure I.2 - Representation of the different types of autophagy	5
Figure I.3 - Pathways leading to the induction of lysosomal membrane permeabilization (LMP)	7
Figure I.4 - Cell death pathways activated after LMP	8
Figure I.5 - Apoptotic-like and necrotic regulated cell death (RCD) in yeast cells	10
Figure I.6 - Assays commonly used in the study of yeast regulated cell death	12
Figure I.7 - Chemical structure of oxazine and its derivatives, phenoxazine and benzo[a]phenoxazine	13
Figure I.8 - Proposed model of Pyridophenoxazine intercalated into the [d(GAA- GCTTC)] ₂ octamer	13
Figure IV.1 - Intracellular distribution of C9 compound	33
Figure IV.2 - Effect of C9 on the viability of <i>Saccharomyces cerevisiae</i> cells in the presence and absence of cycloheximide	34
Figure IV.3 - Effect of C9 in the vacuolar membrane integrity	36
Figure IV.4 - Effect of C9 on cell viability of $\Delta pep4$ mutants	37
Figure IV.5 - Effect of C9 on cell viability of mitochondrial mutants	37
Figure IV.6 - Effect of C9 on cell viability of $\Delta nuc1$, $\Delta aac1/2/3$ and <i>rho</i> ^o mutants	38
Figure IV.7 - Effect of C9 on mitochondrial network	39
Figure IV.8 - Effect of C9 on cell viability of $\Delta yca1$ mutant	40
Figure IV.10 - Effect of C9 on cell viability of autophagic mutants	42
Figure IV.11 - Analysis of Atg8p localization in response to C9 treatment	44
Figure IV.12 - Western blot analysis of GFP-Atg8 processing	45
Figure IV.14 - Analysis of plasma membrane integrity in response to C9	47
Figure VII.1 - Analysis of reactive oxygen species (ROS) accumulation in response to C9 treatment	70
Figure VII.2 - Analysis of plasma membrane integrity in response to C9	72

List of tables

Table 1 – Nile Blue, MSG-111-cd3 and C9 structure and activity against yeast <i>Saccharomyces Cerevisiae</i> PYCC 4072	15
Table 2 - List of <i>Saccharomyces cerevisiae</i> strains used in the present work.	24

Chapter I

Introduction

I. Introduction

I.1 Cell death

There is no life without death. Indeed, cells need to die for the formation and remodeling of biologic structures and tissues, to control the cell number and for the elimination of abnormal cells allowing the normal development and to contribute to homeostasis of different organisms (Baehrecke, 2002). Human diseases as cancer and development disorders can be commonly associated with abnormal regulation of cell death process (Baehrecke, 2002; Fuchs and Steller, 2011).

Until the early years of the 19th century it was though that cell death was inevitable and a passive final stage of life (Fuchs and Steller, 2015). In 1842, Carl Vogt showed that in amphibian metamorphosis the notochord is eliminated facilitating the formation of the vertebrae (Clarke and Clarke, 1996; Fuchs and Steller, 2015). It was the first evidence of development cell death. However, only in the mid 1960's was described for the first time a programmed cell death process dependent on the expression of endogenous genes (Fuchs and Steller, 2015; Lockshin and Williams, 1964). Since then, the field of cell death research showed an increasing progress allowing the discovery and characterization of different subroutines of cell death.

Operationally, cell death can be classified as accidental and regulated. Accidental cell death occurs when the cells are exposed to extreme physicochemical or mechanical stimulus leading to complete and uncontrolled disruption of the cells. In contrast, regulated cell death (RCD) occurs in the context of a failing response to internal or external triggers involving a genetic encoded molecular machinery (Carmona-Gutierrez *et al.*, 2018; Galluzzi *et al.*, 2015). Besides programmed cell death (PCD) which is a physiological instance of RCD associated with development and tissue homeostasis, RCD was firstly classified in three different morphological types such as apoptosis (type I), autophagy (type II) and necrosis (type III) (Galluzzi *et al.*, 2015). Currently, this classification is still accepted but allied with specific biochemical manifestation as well as enzymological criteria (Galluzzi *et al.*, 2012, 2015)

Apoptosis is the most common routine of RCD in eukaryotic cells being involved in several fundamental biological events, and being characterized by defined morphological and biochemical alterations including reduction of cellular volume, chromatin condensation, nuclear fragmentation (karyorrhexis) as well as exposure of phosphatidylserine, which promote phagocytosis by macrophages (Kroemer *et al.*, 2009; Sousa *et al.*, 2012). Apoptotic cells also display little or no

ultrastructural modifications of cytoplasmic organelles and maintain the integrity of the plasma membrane until the final stages of this process (Sousa *et al.*, 2012).

There are two major apoptotic pathways described in mammalian cells, the intrinsic pathway which requires the mitochondrial involvement and is dependent or independent of caspases, and the extrinsic pathway also known as the death receptor pathway where caspases are activated directly (Galluzzi *et al.*, 2012; Sousa *et al.*, 2012). The crucial steps in the mitochondrial pathway which decide the cell fate are the mitochondrial membrane permeabilization (MMP) and caspase activation. The integrity of mitochondrial membrane is regulated by members Bcl-2 protein family. Its permeabilization and consequent release of pro-apoptotic factors like cytochrome c (cyt c), apoptosis inducing factor (AIF), endonuclease G (Endo G), HtrA2/OMI and Smac/DIABLO ensures the propagation of the apoptotic cascade and execution of cell death (Figure 1.1) (Falcone and Mazzoni, 2016; Galluzzi *et al.*, 2012; Sousa *et al.*, 2012).

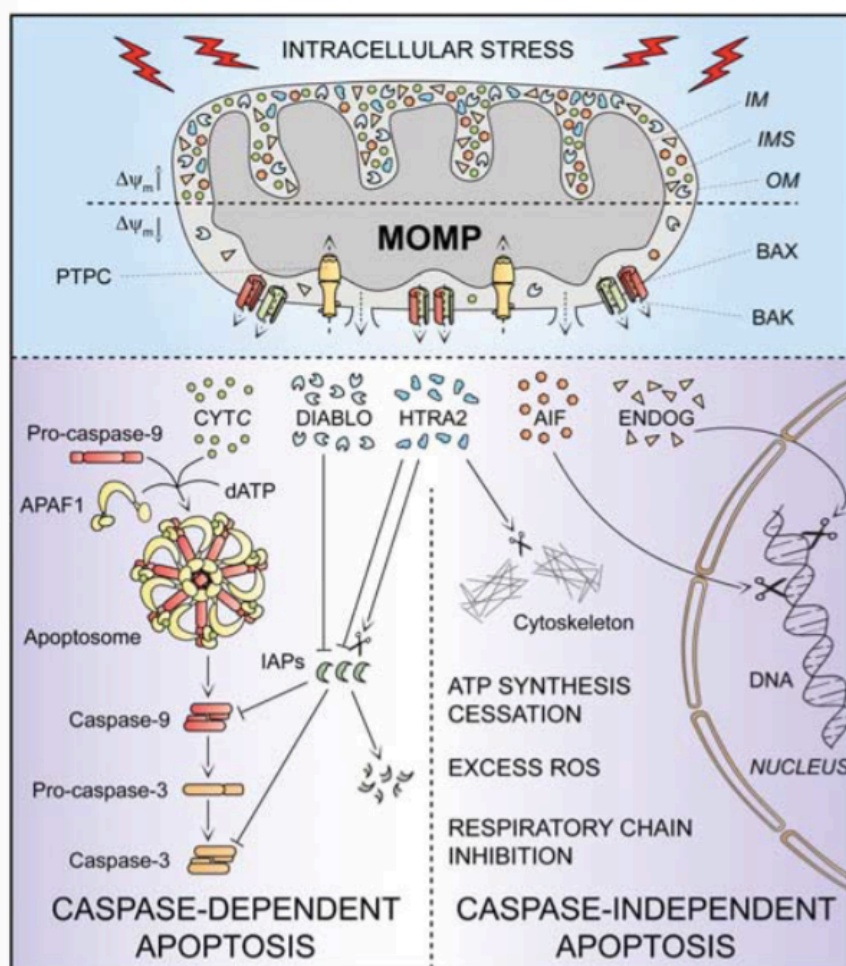


Figure 1.1 – Representation of apoptosis intrinsic pathway which requires the mitochondrial involvement and is dependent or independent of caspases, in response to multiple intracellular stress conditions including DNA damage and cytosolic Ca^{2+} overload (Galluzzi *et al.*, 2012).

Autophagy is a stress-induced catabolic process that is involved in several physiological processes such as cell differentiation, development, adaptation to starvation, the degradation of aberrant structures and life extension (Boya *et al.*, 2013; Chen and Klionsky, 2011). Autophagy can be characterized in three major types, macroautophagy, microautophagy and chaperone-mediated autophagy (Boya *et al.*, 2013; Feng *et al.*, 2014). This process is regulated by conserved autophagy-specific genes (ATG) which have specific functions to control the different steps of the autophagic process (Figure 1.2) (Kroemer and Jäätelä, 2005).

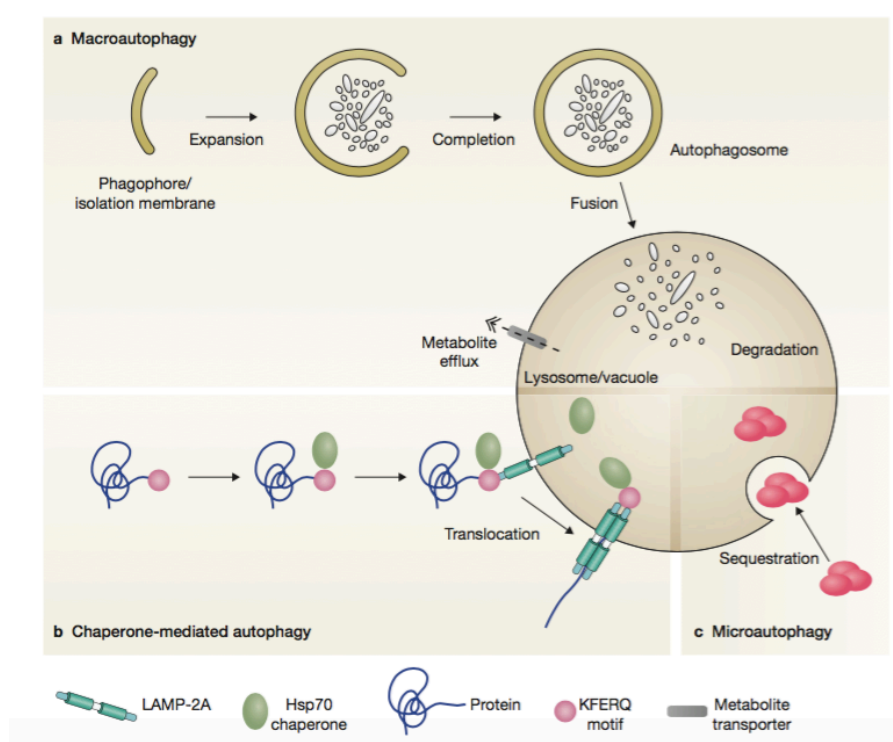


Figure 1.2 – Representation of the different types of autophagy. Macroautophagy **(a)**, chaperone-mediated autophagy **(b)** and microautophagy **(c)** (Boya *et al.*, 2013).

Macroautophagy is a degradative and recycling process that is characterized by the formation of double-membrane vesicles (autophagosomes), where cytoplasmic components like proteins and organelles are sequestered and degraded in the vacuole to generate macromolecules that are released into the cytoplasm for reuse (Carmona-Gutierrez *et al.*, 2018; Falcone and Mazzoni, 2016). The microautophagy also consists in the translocation of cytoplasmic molecules into the lysosome but this time by direct invagination or septation of the lysosomal membrane. The other type involves the binding of Hsp70 (Heat-shock protein 70) chaperones to its cytosolic target, and

then association with the LAMP-2 (lysosomal membrane protein) triggering its oligomerization leading to the translocation of the bound protein into the lysosomal lumen (Feng *et al.*, 2014).

Autophagy constitutes a cytoprotective response which is activated by stressed cells in order to control damage and recycle cell components and its inhibition usually accelerates the cell death. However, when autophagy is excessively induced it can contribute to cell demise (Chen and Klionsky, 2011).

Initially, necrosis has been considered an accidental and uncontrolled form of cell death, that occurs when cells are subjected to an excessive stress. It is now clear that this process can occur in a regulated manner and has an important role in various physiological and pathological settings (Galluzzi *et al.*, 2012; Kroemer *et al.*, 2009). This type of cell death is morphologically characterized by an increase in the cellular volume, swelling of organelles (oncosis), rupture of plasma membrane and release of cytosolic contents as well as chromatin condensation and dilation of nuclear membrane (Galluzzi *et al.*, 2015).

Necrosis can be mediated by several organelles and cellular processes such as mitochondrial alterations, lysosomal and nuclear changes, lipid degradation and increases in the cytosolic concentrations of calcium (Ca^{2+}) (Kroemer *et al.*, 2009). So, depending on the initialization stimuli, such responses can preferentially involve different molecules and organelles leading to specific routines of regulated cell death.

I.1.1 Cell death induced by lysosomal membrane permeabilization

Lysosomes are highly dynamic, membrane-enclosed organelles rich in hydrolytic enzymes that are responsible for the degradation and subsequent recycling of macromolecules derived from the secretory, endocytic, autophagic and phagocytic membrane trafficking pathways (Eskelinen, 2006; Luzio *et al.*, 2007). For many years it was thought that lysosomes were simple “garbage disposals” organelles, however recent studies demonstrated that they are involved in other cellular processes such as metabolism, repair of the plasma membrane, calcium (Ca^{2+}) storage and cell death (Serrano-Puebla and Boya, 2016).

They are filled with several hydrolytic enzymes (proteases, lipases, nucleases, phosphatases, glucosidases, etc.) that usually exert their enzymatic activity at low pH (Kirkegaard and Jäättelä, 2009). Cathepsins are the best characterized proteases being subdivided according to their active site amino acid into cysteine (B, C, H, K, L, O, S, V, W and X/Z), aspartate (D and E) and serine (G) proteases (Kirkegaard and Jäättelä, 2009; Pereira *et al.*, 2015).

The crucial role of the membrane limiting lysosomes is to separate the cellular constituents from unwanted degradation by the hydrolases (Eskelinen, 2006). This membrane contains specific proteins that are implicated in the lysosomal homeostasis and integrity including the lysosomal-associated membrane proteins (LAMP) 1 and 2 which are resistant to hydrolytic digestion and mediate substrate transport, Hsp70 that regulate the protein folding and transport across the membrane as well as vacuolar-type H⁺-ATPases which use metabolic energy derived from ATP to pump protons into the lysosomal lumen to maintain its acidic milieu (Eskelinen, 2006; Serrano-Puebla and Boya, 2016). The lipid composition, such as sphingomyelin levels are also essential for membrane stability (Serrano-Puebla and Boya, 2016).

The lysosomes have emerged as a significant component of the cellular death machinery since lysosomal membrane permeabilization (LMP) causes the release of cathepsins and other hydrolases from the lysosomal lumen to the cytosol which can result in digestion of vital proteins leading to cell death (Boya and Kroemer, 2008).

The type of cell death process is determined by the magnitude of lysosomal permeabilization and consequent amount and type of cathepsins released into the cytosol, the levels of endogenous cathepsins inhibitors such as cystatins as well as the nature of the lethal stimulus (Guicciardi *et al.*, 2004; Sousa *et al.*, 2011). Therefore, massive lysosomal rupture triggered by high intensity stress leads to uncontrolled release of lysosomal contents triggering the cytoplasmic acidification and consequent hydrolysis of its content leading to cell death by necrosis. In contrast, partial and

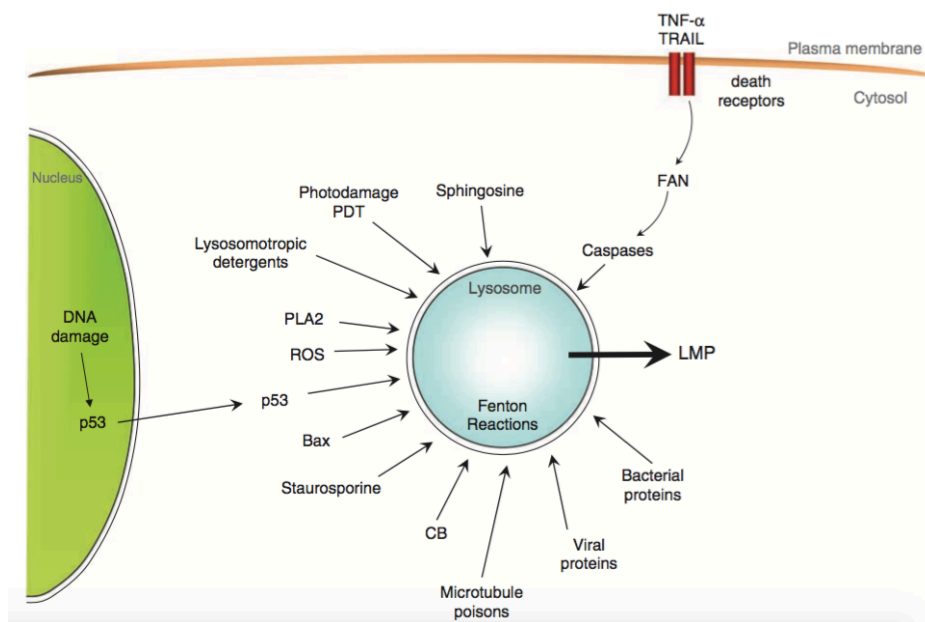


Figure 1.3 – Pathways leading to the induction of lysosomal membrane permeabilization (LMP). LMP can be induced by several agents and molecules such as caspases, bacterial proteins, microtubule poisons, cathepsin B (CB), staurosporine, bax, p53, ROS, lysosomotropic detergents, photodamage by photodynamic therapy (PDT) and sphingosine (Boya and Kroemer, 2008).

selective lysosomal permabilization triggers the regulated cell demise inducing cell death by apoptosis-like cell death (Kirkegaard and Jäättelä, 2009; Serrano-Puebla *et al.*, 2016). LMP can be triggered by distinct agents and molecules including ROS, lysosomotropic agents, endoplasmatic reticulum stress, p53 tumor suppressing protein, endogenous cell death effector Bax, the death receptor of tumor necrosis factor (TNF) receptor family through caspase-8 and FAN which result in cathepsin B release, caspases and cathepsins (Figure I.3) (Boya and Kroemer, 2008; Serrano-Puebla and Boya, 2016).

Among the principal triggers of lysosomal membrane permeabilization are ROS which can induce a fast and direct effect (Blomgran *et al.*, 2007). These molecules pass through the lysosomal membrane and in the presence of free iron can catalyze Fenton reactions to produce toxic intermediates causing peroxidative damage to the proteins in the lysosomal membrane (Blomgran *et al.*, 2007; Serrano-Puebla and Boya, 2016). The lysosomal destabilization leads to cathepsins (B and D) translocation, followed by Bid cleavage by the released proteases and tBid-promoted mitochondrial outer membrane permeabilization with subsequent cytochrome *c* release and caspase-dependent apoptosis (Figure I.4) (Boya and Kroemer, 2008).

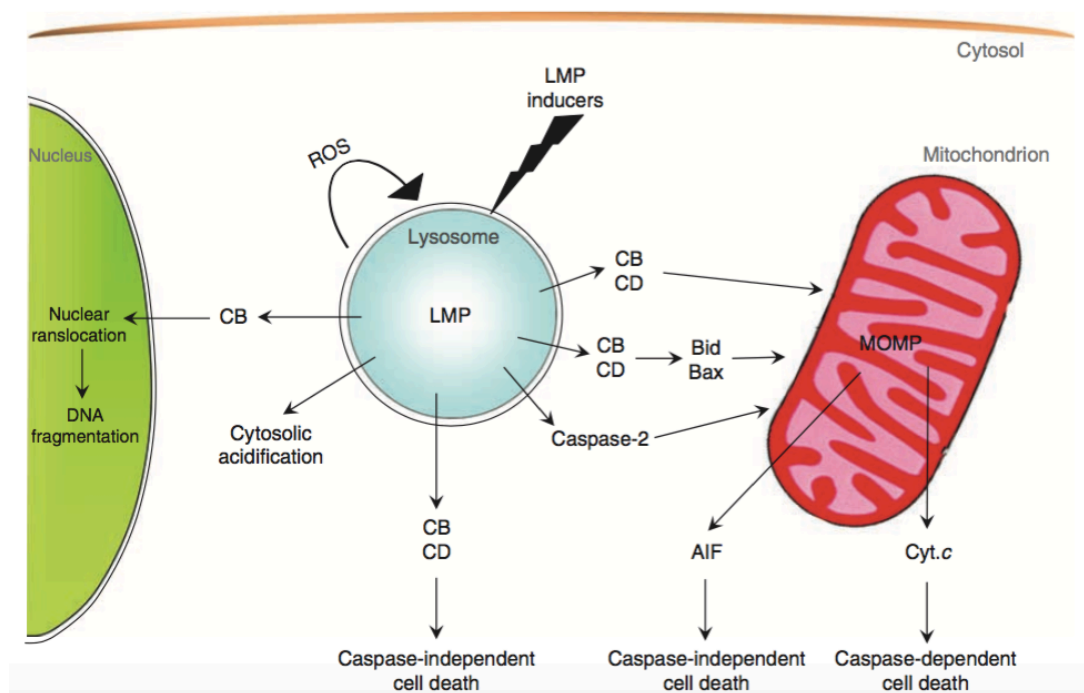


Figure I.4 – Cell death pathways activated after LMP. Different molecules can trigger distinct subroutines of cell death that depend on the intensity of LMP, the expression level of lysosomal hydrolases, the cytosolic concentrations of cathepsin inhibitors, the functional state of mitochondria, the concentration of caspases and their antagonists (Boya and Kroemer, 2008).

Through recent findings, it's now clear that lysosomal proteases such as cysteine cathepsin B and L and aspartate cathepsin D which remain active at neutral pH can cleave some of classic caspase substrates like pro-apoptotic Bcl-2 family proteins indicating that, like caspases also cathepsins are executioners of regulated cell death (Chwieralski *et al.*, 2006; Fehrenbacher *et al.*, 2008). Cathepsin D has been described as a central player in the apoptotic response (Pereira *et al.*, 2015; Sousa *et al.*, 2011), however depending on the stimulus, it can either have an effector or a protective role. In cancer cells it may also have pro-oncogenic effects stimulating angiogenesis, tumor growth, migration and invasion leading to cancer progression (Fehrenbacher *et al.*, 2008; Kirkegaard and Jäättelä, 2009).

Today, is accepted that LMP can trigger distinct cell death pathways involving caspase-dependent or -independent cell death, with or without involvement of mitochondria as well as necrosis and autophagy (Boya and Kroemer, 2008; Guicciardi *et al.*, 2004; Sousa *et al.*, 2011).

I.2 Yeast cell death

Nowadays the yeast *Saccharomyces cerevisiae* is one of the most used and versatile eukaryotic cell models (Sousa *et al.*, 2012). Due to its easy genetic manipulation and maintenance, yeast is a useful model to study complex scenarios of stress response, longevity and regulated cell death (Carmona-Gutierrez *et al.*, 2010; Falcone and Mazzoni, 2016; Ring *et al.*, 2012).

Since the first evidences suggesting that yeast presented endogenous programmed cell death displaying typical markers of apoptosis (Madeo *et al.*, 1997), the reason why unicellular organisms would commit suicide has been questioned. Microorganisms like yeast and bacteria can switch from unicellular to multicellular organization such as colonies, biofilms and aggregates to increase the genetic diversity and the protection against hostile environments (Allocati *et al.*, 2015; Carmona-Gutierrez *et al.*, 2018). It is now clear that unfitted, damaged and old cells from a multicellular organization can commit suicide promoting the survival of the population in several physiological contexts including antagonistic interactions between yeasts, aging, mating and colony formation (Büttner *et al.*, 2006; Carmona-Gutierrez *et al.*, 2018).

The knowledge of the full *Saccharomyces cerevisiae* genome sequence has revealed a high degree of conservation between protein amino acid sequence and function in yeast and higher eukaryotic species (Duina *et al.*, 2014) leading to the uncovering of new genes and pathways that regulate physiological and pathological processes (Falcone and Mazzoni, 2016; Sousa *et al.*, 2012).

As previously mentioned in mammalian, yeast regulated cell death (RCD) such as apoptosis, necrosis and autophagy-dependent cell death can be triggered by distinct internal and external stimuli (Figure I.5) (Falcone and Mazzoni, 2016).

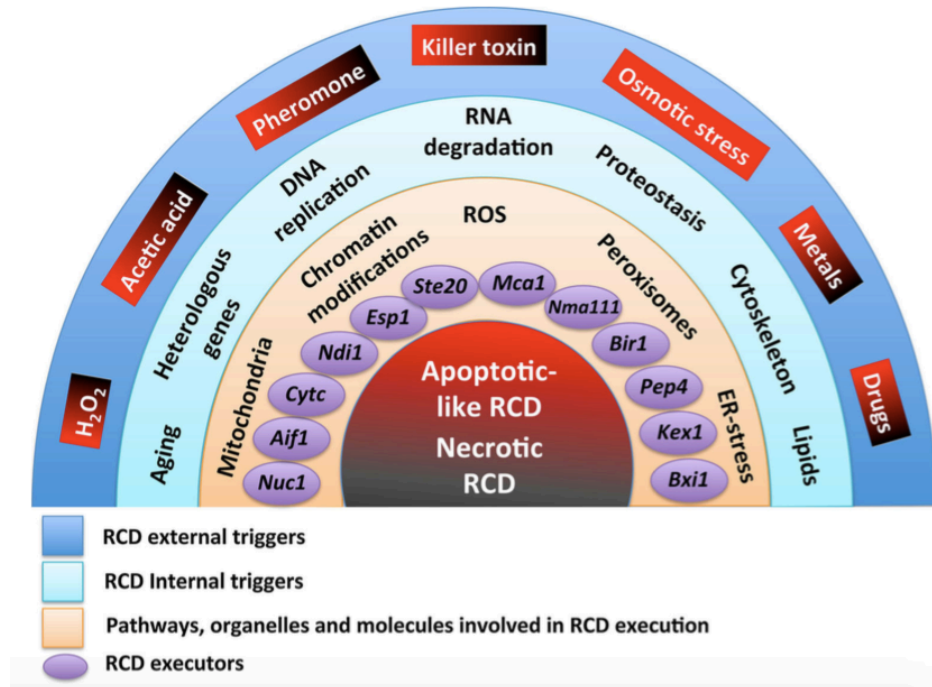


Figure I.5 – Apoptotic-like and necrotic regulated cell death (RCD) in yeast cells. Internal and external triggers, pathways, organelles and molecules involved in RCD execution.

RCD can be induced by alterations in fundamental cellular pathways including DNA replication, mRNA stability, protein modification and degradation as well as accumulation of ROS, aging and the heterologous expression of pro-apoptotic human genes such as Bax and p53 (Carmona-Gutierrez *et al.*, 2010; Falcone and Mazzoni, 2016; Ludovico *et al.*, 2005). Recent studies demonstrated that the expression of p53 induces apoptosis-like cell death (Falcone and Mazzoni, 2016). Also, several triggers can induce RCD in yeast including hydrogen peroxide (H_2O_2), acetic acid, osmotic stress, high salt concentration, drugs and others (Falcone and Mazzoni, 2016). Depending in their concentrations different cell death pathways can be induced.

As for mammalian, yeast cell death also displays characteristic morphological features such as DNA fragmentation, ROS accumulation, chromatin condensation, exposure of phosphatidylserine on the cell surface, mitochondrial outer membrane permeabilization with cyt c release (Falcone and Mazzoni, 2016; Mazzoni and Falcone, 2008). This process is regulated by several yeast orthologous of mammalian apoptotic regulators including the yeast metacaspase, Yca1p, which displays both pro-apoptotic and anti-apoptotic functions (Falcone and Mazzoni, 2016;

Mazzoni and Falcone, 2008), yeast apoptosis inducing factor (Aif1p) (Chin *et al.*, 2014), yeast Nuc1p (ortholog of mammalian Endonuclease G) and cytochrome *c* (cyt *c*) that are released from mitochondria in response to apoptotic stimuli, among others (Figure 1.5) (Pereira *et al.*, 2008; Falcone and Mazzoni, 2016; Mason *et al.*, 2005).

During apoptosis, an increased permeabilization of organelle membranes can occur, such as mitochondrial outer membrane permeabilization and lysosomal membrane permeabilization (Mason *et al.*, 2005). The permeability of yeast vacuoles, which are the yeast equivalent to mammalian lysosomes, is also involved in the regulation of apoptotic-like cell death (Li and Kane, 2009; Rodrigues *et al.*, 2013). Studies indicate that the translocation of vacuolar protease Pep4p leads to the degradation of damaged mitochondria through an autophagic-independent process displaying a protective role in acetic acid-induced cell death (Pereira *et al.*, 2010). Similar results were observed in colorectal carcinoma cells where the cathepsin D is released by lysosomal permeabilization, protecting the cells from mitochondrial dysfunction through its involvement in degradation of damaged mitochondria in acetate-induced apoptosis (Marques *et al.*, 2013).

The evidences above mentioned, reinforce the use of yeast as a suitable model to study the different organelles and molecules involved in regulated cell death process.

There are many assays and tools available that can be used to evaluate and characterize the mechanism underlying the cell death process in response to specific stressor. Thus, in a first phase, it is important to determine the cell survival through clonogenic assays which reflects the ability of a cell to divide when exposed to that trigger, usually assessed by quantification of Colony Formation Units (CFU). Similarly, the evaluation of the physiological state (vitality) should be performed, either by determination of the cellular ATP content, mitochondrial membrane potential or esterase activity (Carmona-Gutierrez *et al.*, 2010; Kwolek-Mirek and Zdrag-Tecza 2014).

The different routines of cell death display characteristic features which can be used to identify the death phenotype. In apoptotic cells, morphological and biochemical changes as DNA fragmentation, chromatin condensation and ROS accumulation can be evaluated by TUNEL (terminal deoxynucleotidyl transferase dUTP nick end-labeling), DAPI and dihydroethidium (DHE) staining, respectively (Carmona-Gutierrez *et al.*, 2010; Carmona-Gutierrez *et al.*, 2018). To distinguish necrotic cells from apoptotic cells Annexin V staining combined with propidium iodide (PI) staining can be used. In this double staining method, early apoptotic cells exhibit AnnV+/PI- staining indicative of phosphatidylserine externalization, primary necrotic cells exhibit AnnV-/PI+ staining indicative of plasma membrane rupture, while late apoptotic/secondary necrotic cells

display AnnV+/PI+ staining indicating both PS externalization and membrane permeabilization (AnnV+/PI+) (Figure I.6) (Carmona-Gutierrez *et al.*, 2010; Carmona-Gutierrez *et al.*, 2018).

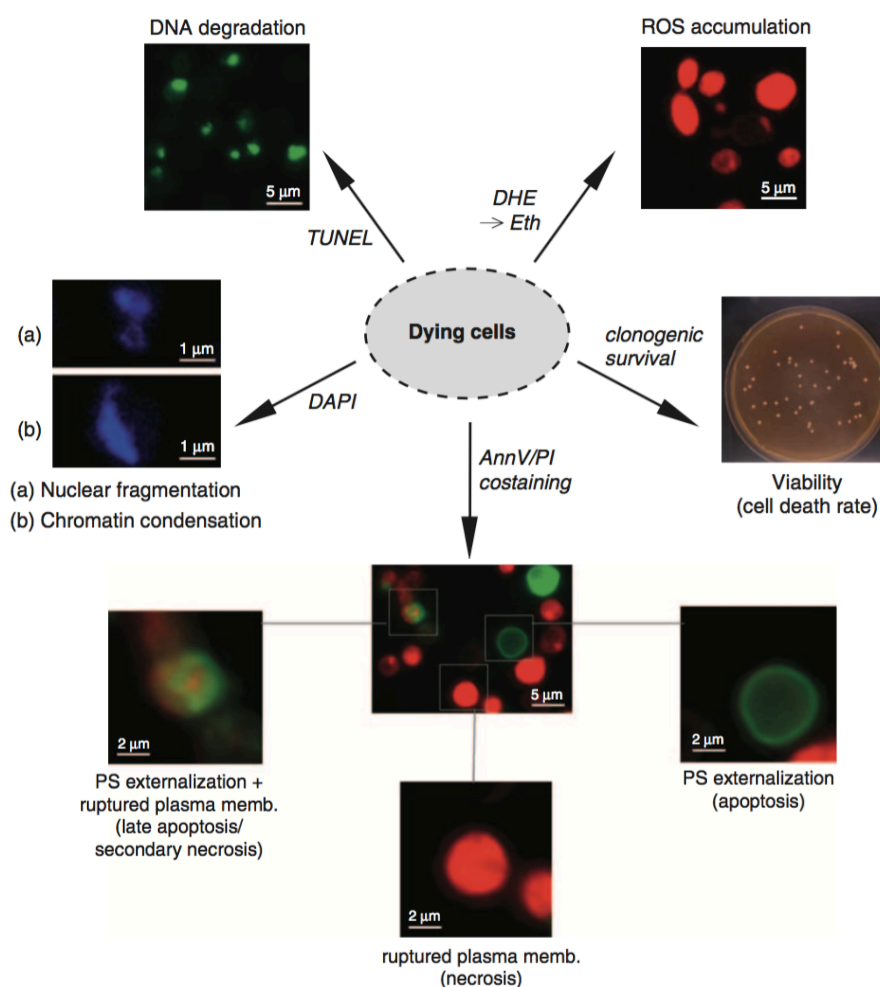


Figure I.6 – Assays commonly used in the study of yeast regulated cell death. Clonogenic assays are used to evaluate cell death rates. DAPI staining is used to observe chromatin condensation and nuclear fragmentation, while TUNEL is used to identify DNA fragmentation. Co-staining of Annexin V and propidium iodide (PI) allows the distinction between early apoptotic (AnnV+/PI-) from late apoptotic and secondary necrotic (AnnV+/PI+) as well as primary necrotic cells (AnnV-/PI+). In all the cases stained cells are usually analyzed by flow cytometry and/or fluorescence microscopy observations (Carmona-Gutierrez *et al.*, 2010).

I.3 Phenoxazine and benzophenoxazine derivatives

Fluorescent chromophores have been the subject of an increasing research because of their application in detection and labelling of biomolecules (Frade *et al.*, 2005). This growing interest, has boosted the creation of new selective fluorescent biomarkers with photostable properties that can absorb and emit in the red and near infrared (NIR) spectral regions (600-1000 nm), minimizing the undesirable biomolecular autofluorescent background signals (Frade *et al.*, 2005; Song *et al.*, 2008).

Long wavelength fluorophores like oxazine and its derivatives which acts as tunable laser dyes in the range 600–900 nm (Frade *et al.*, 2008), have been commonly used in non-covalent labeling of nucleic acids in blotting experiments, electrophoretic gels and living cell assays (Soto *et al.*, 2002) as well as in covalent labelling of carboxylic acids, proteins, peptides, aminoacids, DNA (Frade *et al.*, 2008).

Besides their photophysical properties, phenoxazine and benzo[*a*]phenoxazine dyes which derived from the oxazine heterocycle (Figure I.7), also possess an interesting antiproliferative activity (Frade *et al.*, 2008). Several studies demonstrated that these compounds display a wide spectrum of biological activities as antitumour (Bolognese *et al.*, 2006; Shimamoto *et al.*, 2001), antimicrobial (Patil *et al.*, 2015), antiviral (Iwata *et al.*, 2005), anti-inflammatory (Silva *et al.*, 2004) and antifungal activity (Kumar *et al.*, 2006).

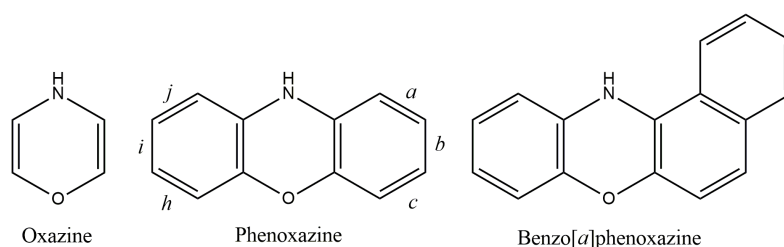


Figure I.7 - Chemical structure of oxazine and its derivatives, phenoxazine and benzo[*a*]phenoxazine.

These compounds are typically DNA-intercalating agents due to the ability of their large planar polycycle structure to intercalate between specific base pairs through hydrogen bonds and π - π stacking interactions leading to the formation of stable DNA/compound complex (Figure I.8) (Bolognese *et al.*, 2002a; Bolognese *et al.*, 2002b). The intercalative binding can disrupt the normal DNA function through enzymatic blocking, reading errors and metabolic conversion to free radicals leading to cell death (Alberti *et al.*, 2003; Bolognese *et al.*, 2002a; Frade *et al.*, 2008).

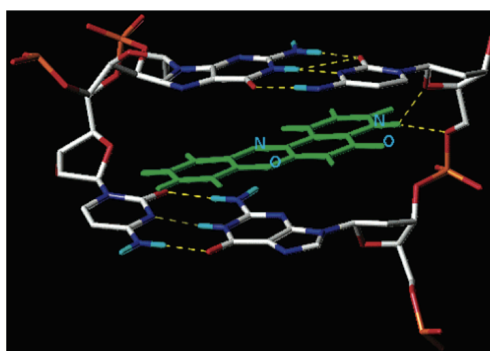


Figure I.8 - Proposed model of Pyridophenoxazine intercalated into the [d(GAA- GCTTC)]₂ octamer. Dashed lines represent hydrogen bonds (Alberti *et al.*, 2003).

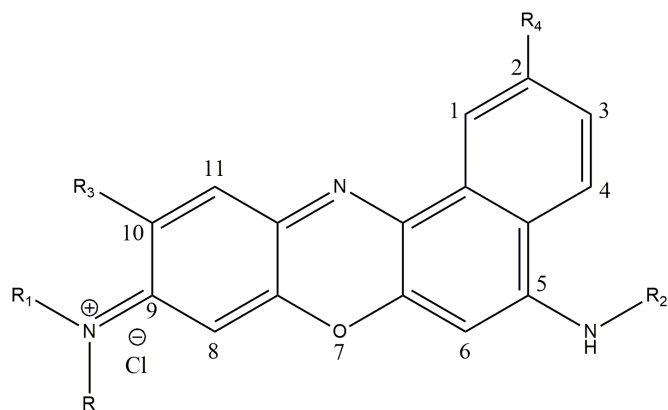
The phenoxazine nucleus is common to many natural and synthetic compounds associated with anticancer activity as in the case of Actinomycin D, one of the most well-known chemotherapeutic drugs. The antitumor activity of these compounds seems to be due specifically to the presence of the phenoxazine structure, which by intercalating in DNA can inhibit the DNA-dependent RNA polymerase (Alberti *et al.*, 2003; Wesolowska *et al.*, 2006). Phenoxazine derivatives can also be effective modulators of multidrug resistance in P-glycoprotein overexpression T lymphoma cells (Wesolowska *et al.*, 2006).

The enormous potentialities and applications of phenoxazine derivatives, led our group to synthesized new benzo[*a*]phenoxazine using as a lead compound one of the most common compound in this family, the Nile blue. Previous studies demonstrated that the newly synthesized compounds can be used as antifungal agents, in particular the MSG-111-cd3 that exhibited high antifungal activity against the yeast *Saccharomyces cerevisiae* as a model (Carvalho, 2011 ;Frade *et al.*, 2007). Co-localization studies showed that at concentrations close to the minimum inhibitory concentration (MIC), MSG-111-cd3 accumulates in the vacuolar membrane and in the membrane of endoplasmic reticulum (Leitão, 2015). So far, the studies indicate that MSG-111-cd3 induces a regulated process mediated by the vacuolar permeabilization with a prominent role of Pep4p. The treatment did induce the release of Nhp6Ap (yeast ortholog of the mammalian HMGB1), however no loss of plasma membrane integrity was observed, so a necrotic cell death process does not seem to be induced. Also the autophagy and the mitochondrial pathway do not seem to be involved in the cell death process (Ferreira, 2017; Lopes, 2015).

In this work, we investigated the molecular mechanism of cell death induced by a benzo[*a*]phenoxazine compound with similar structure to MSG-111-cd3 compound to further understand the structure-activity relationships of the benzo[*a*]phenoxazine compounds synthesized by our group.

N-(10-methyl-5-(propylamino)-9*H*-benzo[*a*]phenoxazin-9-ylidene)ethanaminium chloride, also designated as C9, presents a benzene ring fused with the *a* face of the phenoxazine structure (Figure 1.7). As Nile blue and MSG-111-cd3 compounds, C9 presents an amine functional group at the position 5 of the system (Table 1) that is essential for covalent labelling molecules but also confer them the possibility of other chemical modifications (Frade *et al.*, 2008). Structurally, C9 differs from the MSG-111-cd3 in R₂ substituent, where presents a propyl group rather than 4-ethoxy-4-oxobutyl which increases their antifungal activity (Leitão, 2015).

Table 1 – Nile Blue, MSG-111-cd3 and C9 structure and activity against yeast *Saccharomyces cerevisiae* PYCC 4072 (Leitão, 2015).



Compound	R	R ₁	R ₂	R ₃	R ₄	MIC/ μ M
Nile Blue	CH ₂ CH ₃	CH ₂ CH ₃	H	H	H	25.0
MSG-111-cd3	CH ₂ CH ₃	H	(CH ₂) ₃ CO ₂ Et	CH ₃	H	25.0
C9	CH ₂ CH ₃	H	(CH ₂) ₂ CH ₃	CH ₃	H	6.25

Chapter II

Aims

II. Aims

Due to its remarkable properties previously described, the yeast *Saccharomyces cerevisiae* represents a unique eukaryotic model to study complex scenarios of stress response, longevity and cell death (Ring *et al.*, 2012).

Previous studies in our group using the yeast *Saccharomyces cerevisiae* as a model showed that a newly synthesized benzo[a]phenoxazine compound (MSG-111-cd3) exhibited high antifungal activity. So, based on its activity our group studied the mechanism underlying the effect of MSG-111-cd3 compound. It was observed that this compound induces a regulated cell death process which may be mediated through the permeabilization of the vacuolar membrane, without the involvement of autophagy and mitochondrial pathways (Ferreira, 2017; Lopes, 2015).

The interesting potential of newly benzo[a]phenoxazine compounds lead us to study a compound of this family (C9) that differ from MSG-111-cd3 only in a single substitution of its extended aromatic system which considerably increases its antifungal activity.

To characterize the intracellular distribution and the cell death mechanism induced by C9 compound fluorescence microscopy, flow cytometry and cell viability assays were used to assess several death markers including plasma membrane integrity, accumulation of reactive oxygen species (ROS), detection of a sub G0/G1 peak, mitochondrial network fragmentation, vacuolar membrane permeabilization as well as the autophagy involvement. For this characterization, various strains deficient in proteins reported to be involved in different subroutines of cell death, and strains expressing specific fluorescent proteins to visualize different organelles and cellular alterations were also used.

Chapter III

Material and Methods

III. Material and Methods

III.1 Yeast strains

The *Saccharomyces cerevisiae* strains used in this study are listed in Table 2. As wild type strains were used BY 4741, W303-1A and W303-1B. BY 4741 WT, BY 4741 $\Delta pep4$, BY 4741 $\Delta cpr3$, BY 4741 $\Delta aif1$, BY 4741 $\Delta nuc1$, BY 4741 $\Delta yca1$, BY 4741 rho^o , W303-1A WT, W303-1A $\Delta pep4$, W303-1A GFP-ATG8, W303-1A $\Delta atg1$ GFP-ATG8, W303-1A $\Delta atg5$ GFP-ATG8, W303-1A $\Delta atg32$ GFP-ATG8, W303-1B and JL1-3 $\Delta aac1/2/3$ were used in cell viability assays.

For fluorescence microscopy assays BY 4741 WT, W303-1A GFP-ATG8, W303-1A $\Delta atg1$ GFP-ATG8, W303-1A $\Delta atg5$ GFP-ATG8, W303-1A $\Delta atg32$ GFP-ATG8 and W303-1A pYX-mt-GFP were used. For flow cytometry only BY 4741 was used.

III.2 Media and growth conditions

Yeast cells, BY 4741 WT, BY 4741 $\Delta pep4$, BY 4741 $\Delta cpr3$, BY 4741 $\Delta aif1$, BY 4741 $\Delta nuc1$, BY 4741 $\Delta yca1$, BY 4741 rho^o , BY4741 GFP-SEC66, W303-1A WT and W303-1A $\Delta pep4$ were grown on YEPDA (Yeast Extract Peptone Dextrose) medium plates (1% yeast extract, 2% bactopectone, 2% glucose and 2% agar) at 30 °C during 2-3 days. Then, they were transferred to liquid YEPD (YPDA without agar) at 30 °C in an orbital shaker at 200 rpm, with a ratio of flask volume/medium of 5:1 and allowed to reach the exponential phase ($OD_{640nm} \approx 0.5-0.6$).

Strains transformed with plasmids, W303-1A GFP-ATG8, W303-1A $\Delta atg1$ GFP-ATG8, W303-1A $\Delta atg5$ GFP-ATG8, W303-1A $\Delta atg32$ GFP-ATG8, W303-1A pDF01-VBA1-YEGFP and W303-1A pYX-mt-GFP were grown in synthetic complete medium (SC: 2% glucose, 0.5% (w/v) ammonium sulphate, 0.7% yeast nitrogen base w/o amino acids, 0.2% dropout mix, 0.01% histidine, uracil and tryptophan, 0.02% leucine) but without the appropriate amino acids. In the strain carrying a pYX-mt-GFP plasmid, 2% galactose instead of glucose was used for induction the expression of the proteins. All the strains were growth at 30 °C with agitation at 200 rpm, until they reach the exponential phase ($OD_{640nm} \approx 0.5-0.6$).

Table 2 - List of *Saccharomyces cerevisiae* strains used in the present work.

Yeast strain	Genotype	Source
BY 4741	MATa, <i>his3Δ1</i> , <i>leu2Δ0</i> , <i>met15Δ0</i> , <i>ura3Δ0</i>	EUROSCARF
W303-1A	MATa, <i>ura3-52</i> , <i>trp1Δ2</i> , <i>leu2-3</i> , <i>112 his3-11</i> , <i>ade2-1</i>	EUROSCARF
W303-1B	MATa, <i>ade2</i> , <i>his3</i> , <i>leu2</i> , <i>trp1</i> , <i>ura3</i> , <i>can1</i>	Alexander Tzagoloff
BY 4741 $\Delta pep4$	MATa, <i>his3Δ1</i> , <i>leu2Δ0</i> , <i>met15Δ0</i> , <i>ura3Δ0</i> ; <i>YPL154c::kanMX4</i>	EUROSCARF
BY 4741 $\Delta cpr3$	MATa; <i>ura3Δ0</i> ; <i>leu2Δ0</i> ; <i>his3Δ1</i> ; <i>met15Δ0</i> ; <i>YML078w::kanMX4</i>	EUROSCARF
BY 4741 $\Delta aif1$	MATa; <i>ura3Δ0</i> ; <i>leu2Δ0</i> ; <i>his3Δ1</i> ; <i>met15Δ0</i> ; <i>YNR074c::kanMX4</i>	EUROSCARF
BY 4741 $\Delta nuc1$	MATa; <i>ura3Δ0</i> ; <i>leu2Δ0</i> ; <i>his3Δ1</i> ; <i>met15Δ0</i> ; <i>YJL208c::kanMX4</i>	EUROSCARF
BY 4741 $\Delta yca1$	MATa; <i>ura3Δ0</i> ; <i>leu2Δ0</i> ; <i>his3Δ1</i> ; <i>met15Δ0</i> ; <i>YOR197w::kanMX4</i>	EUROSCARF
BY 4741 <i>rho^o</i>	MATa, <i>his3Δ1</i> , <i>leu2Δ0</i> , <i>met15Δ0</i> , <i>ura3Δ0 rho^o</i>	This study
BY 4741 GFP-SEC66	MATa, <i>his3Δ1</i> , <i>leu2Δ0</i> , <i>met15Δ0</i> , <i>ura3Δ0</i>	Brian Zid
W303-1A $\Delta pep4$	MATa, <i>ura3-52</i> , <i>trp1Δ2</i> , <i>leu2-3</i> , <i>112 his3-11</i> , <i>ade2-1 YPL154c::kanMX4</i>	(Pereira, 2015)
W303-1A GFP-ATG8	MATa, <i>ura3-52</i> , <i>trp1Δ2</i> , <i>leu2-3</i> , <i>112 his3-11</i> , <i>ade2-1</i> , GFP-ATG8 (URA3)	Nadine Camougrand
W303-1A $\Delta atg1$ GFP-ATG8	MATa, <i>ura3-52</i> , <i>trp1Δ2</i> , <i>leu2-3</i> , <i>112 his3-11</i> , <i>ade2-1</i> , <i>YGL180w::kanMX4</i> , GFP-ATG8 (URA3)	Nadine Camougrand
W303-1A $\Delta atg5$ GFP-ATG8	MATa, <i>ura3-52</i> , <i>trp1Δ2</i> , <i>leu2-3</i> , <i>112 his3-11</i> , <i>ade2-1</i> , <i>YPL149w::kanMX4</i> , GFP-ATG8 (URA3)	Nadine Camougrand
W303-1A $\Delta atg32$ GFP-ATG8	MATa, <i>ura3-52</i> , <i>trp1Δ2</i> , <i>leu2-3</i> , <i>112 his3-11</i> , <i>ade2-1</i> , <i>YIL146c::kanMX4</i> , GFP-ATG8 (URA3)	Nadine Camougrand
W303-1A pYX-mt-GFP	MATa, <i>ura3-52</i> , <i>trp1Δ2</i> , <i>leu2-3</i> , <i>112 his3-11</i> , <i>ade2-1</i> , pYX-mt-GFP (URA3)	Nadine Camougrand
W303-1A pDF01-VBA1-YEGFP	MATa, <i>ura3-52</i> , <i>trp1Δ2</i> , <i>leu2-3</i> , <i>112 his3-11</i> , <i>ade2-1</i> , pDF01-VBA1-YEGFP (URA3)	Josef Nosek
JL1-3 $\Delta aac1/2/3$	MATa, <i>ade2</i> , <i>his3</i> , <i>leu2</i> , <i>trp1</i> , <i>ura3</i> , <i>can1</i> , <i>aac1::LEU2</i> , <i>aac2::HIS3</i> , <i>aac3::URA3</i>	(Postis <i>et al.</i> , 2005)

III.3 C9 stock solution preparation and treatment

N-(10-methyl-5-(propylamino)-9H-benzo[a]phenoxazin-9-ylidene)ethanaminium chloride (C9) was dissolved in dimethyl sulfoxide (DMSO) to a final concentration of 19.625 mM.

As previously described the yeast cells were grown in their respective liquid media at 30 °C with agitation at 200 rpm, until they reach the exponential phase ($OD_{640nm} \approx 0.5-0.6$). After, that the cells were collected, centrifuged for 3 minutes at 5000 rpm and resuspended in PBS 1x (10x: 80.6 mM Na_2HPO_4 , 19.4 mM KH_2PO_4 , 1.37 M NaCl, 27 mM KCl).

The C9 treatment was performed by adding C9 to the resuspended cells at final concentration of 7.5 μ M. The same volume of DMSO ($\approx 0.038\%$) was added to another tube that served as negative control. Incubation took place for 120 min at 30 °C with agitation at 200 rpm. Cells were collected every 30 minutes along 120 minutes, the 0 minutes sample was collected before adding the compound and DMSO.

III.4 Production of BY 4741 rho⁰ strain

Cells were grown in YEPD overnight at 30 °C with agitation at 200 rpm. After that the cells were collected at an $OD_{640nm} \approx 2$, resuspended in fresh YEPD medium and supplemented with 25 μ g ml⁻¹ Ethidium bromide (Sigma-Aldrich). After incubation for 7 days at 30°C with shaking, the cells were plated on YEPDA in different dilutions (10^{-3} , 10^{-4} , 10^{-5} , and 10^{-6}) and grown at 30°C for 2-3 days. Then the cells were replicated both in YEPDA and YEPGA (1% yeast extract, 2% bacto-peptone, 2% glycerol and 2 % agar).

Colonies that grew on YEPDA plates and did not grow on YEPGA plates were selected and the rho⁰ phenotype was confirmed by Polymerase Chain Reaction (PCR) for detection of the COX2 gene.

III.5 Cell viability assays and proteins synthesis inhibition

Before (time zero) and after adding the C9 and DMSO (negative control) samples of 50 μ L of culture were collected every 30 min along 120 minutes and diluted 10^{-4} in sterile deionized water. 30 μ L from the 10^{-4} dilution were inoculated onto YEPDA plates and colony-forming units (CFU) were counted after 2-3 days of incubation at 30 °C. The cell viability was estimated considering 100% survival the number of CFU obtained at time zero.

For protein synthesis inhibition assays, the cells were incubated with cycloheximide (CHX) (Sigma-Aldrich) and absolute ethanol (negative control) for 30 minutes before C9 and DMSO treatment. Cycloheximide was dissolved in absolute ethanol and added to cells at a final concentration of 100 $\mu\text{g ml}^{-1}$ after they reach the exponential phase ($\text{OD}_{640\text{nm}} \approx 0.5-0.6$).

III.6 Assessment of C9 intracellular distribution

To confirm the preferential localization of the C9 compound, co-localization experiments were performed using *Saccharomyces cerevisiae* strains expressing GFP-tagged proteins that localize to specific intracellular organelles. BY4741 GFP-SEC66 and W303-1A pDF01-VBA1-YEGFP cells were treated with C9 and visualized by epifluorescence microscopy.

III.7 Assessment of plasma membrane integrity

Integrity of the plasma membrane was assessed by flow cytometry using the impermeable dye propidium iodide (PI) (Sigma).

BY 4741 cells were treated with C9 or DMSO (negative control) as described in II.3. Samples of 200 μL of cell culture were collected at specific time points (0, 15, 30, 60, 90 and 120 minutes), centrifuged for 3 minutes at 5000 rpm, resuspended in 500 μL PBS 1x and incubated with 2 $\mu\text{g ml}^{-1}$ of PI for 10 minutes at room temperature in the dark. As a positive control for PI staining boiled cells were used.

III.8 Assessment of vacuole membrane permeabilization

In order to assess the vacuole membrane permeabilization, BY 4741 cells were treated with C9 or DMSO (negative control) as described in II.3.

Samples of cell culture were collected at specific time points (0, 30, 60, 90 and 120 minutes) and incubated with Celltracker™ Blue CMAC (Molecular Probes Eugene, USA) at a final concentration of 2 μM for 20-30 minutes at room temperature. Then, the cells were visualized by epifluorescence microscopy.

III.9 Assessment of mitochondrial network fragmentation

Fragmentation of mitochondrial network was assessed using W303-1A cells transformed with a plasmid expressing a mitochondrial GFP (pYX-mtGFP). After treatment with C9 and DMSO

(negative control) as described in II.3, the cells were collected at specific time points (0, 30, 60, 90 and 120 minutes) and visualized by epifluorescence microscopy.

III.10 Assessment of the accumulation of reactive oxygen species

Intracellular superoxide anion was quantified by flow cytometry using dehydroethidium (DHE) (Sigma) probe to assess the accumulation of reactive oxygen species (ROS).

Samples of 200 μL of cell culture were collected at specific time points (0, 15, 30, 60, 90 and 120 minutes), before and after the treatment with C9 and DMSO (negative control). Then were centrifuged for 3 minutes at 5000 rpm, resuspended in 500 μL PBS 1x and incubated with 2 $\mu\text{g ml}^{-1}$ of DHE for 20 minutes at room temperature in the dark. As a positive control for DHE staining treatment with hydrogen peroxide (H_2O_2) was used.

III.11 Cell cycle analysis

Cell cycle distribution and detection of a sub-G0/G1 population were assessed by flow cytometry.

BY 4741 cells were treated with C9 or DMSO (negative control) as described in II.3. Samples of 500 μL of cell culture were collected at specific time points (0, 15, 30, 60, 90 and 120 minutes) and fixed in 500 μL of 70% ethanol (EtOH) overnight at 4 $^\circ\text{C}$. Then, the cells were washed in 50 mM sodium citrate buffer (pH 7.5) and resuspended in 450 μL of the same buffer, followed by a 60 minutes incubation with 0.25 mg ml^{-1} of RNAse A (in Tris-EDTA, pH 8) (Sigma) and another 60 minutes incubation with 1 mg ml^{-1} of Proteinase K (in H_2O) (NZytech, Portugal), both at 50 $^\circ\text{C}$. 2 μL of 5mM SYTOX Green (10x diluted in Tris-EDTA, pH 8) was added to 100 μL of each sample and incubated overnight at 4 $^\circ\text{C}$. After the addition of Triton X-100 (0.25% (v/v) in sodium citrate buffer pH 7.5) and to reduce cell aggregates, the final suspension was sonicated with 3 pulses of 30 W for 1-2 seconds each.

III.12 Assessment of autophagy induction

W303-1A GFP-ATG8, W303-1A $\Delta atg1$ GFP-ATG8, W303-1A $\Delta atg5$ GFP-ATG8 and W303-1A $\Delta atg32$ GFP-ATG8 cells were treated with C9 and DMSO (negative control) as previously described in II.3. As a positive control for autophagy induction, cells were incubated with rapamycin at a final concentration of 0.2 $\mu\text{g ml}^{-1}$ at 30 $^\circ\text{C}$ with agitation.

III.12.1 GFP-Atg8 protein localization

To assess the GFP-Atg8 protein localization, the cells were collected before and after 60 minutes of treatment with C9, DMSO (negative control) and rapamycin (positive control). Then, cells were visualized by epifluorescence microscopy.

III.12.2 Western blot analysis

Western blot analysis was performed to evaluate the GFP-Atg8 processing. First, 1 ml of cell culture was collected before and after 60 minutes of treatment with C9, DMSO (negative control) and rapamycin (positive control).

To prepare the protein extracts, cells were resuspended in 500 μ l deionized water and added 50 μ l of 3.5% (v/v) β -mercaptoethanol in 2M NaOH solution. After vortexing and incubation for 15 minutes on ice, 50 μ l of 50 % trichloroacetic acid (TCA) were added. Then, the samples were again vortexed and incubated for 15 minutes on ice followed by a centrifugation at 15000 rpm for 10 minutes at 4 °C. The pellet was resuspended in 60 μ l of *Laemmli* Buffer 1x (4x: 0.25 M Tris-HCl, 9.2% (w/v) SDS, 40% (w/v) glycerol, 5% (w/v) β -mercaptoethanol, 0.5% (w/v) bromophenol blue) and 1.5 μ l of 1M Tris pH 9.5 were added to maintain the ideal pH and the blue colour. Finally, the extracts were denatured at 95 °C for 5 minutes and stored in -20 °C until Western blot analysis.

The protein extracts were separated by SDS Polyacrylamide Gel Electrophoresis (SDS-PAGE) with 15% of polyacrylamide gels on a Mini Protean III electrophoresis system (BioRad) at a constant amperage (20 mA per gel) for 60 to 90 minutes using running buffer 1x (10x: 0.25 M Tris base, 1.92 M Glycine, 1% SDS). As reference for molecular weight the NZY Colour Protein Marker II was used. Proteins were transferred from the gel to the polyvinylidene fluoride (PVDF) membrane (Hybond-ECL, GE Healthcare) in a semi-dry transfer unit (TE77X Hoefer) at 60 mA during 90 minutes using transfer buffer 1x (10x: 0.25 M Tris-Base, 1.92 M glycine). The membranes were blocked in 5% (w/v) non-fat milk dissolved in PBS-T (PBS 1x, 0,05% (v/v) Tween 20) for 90 minutes at room temperature with agitation to avoid non-specific interactions. Then, they were incubated with the primary antibody overnight at 4 °C, washed with PBS-T for 15 minutes (4x) followed by the incubation with the secondary antibody for 60 minutes at room temperature.

The primary antibodies used were mouse monoclonal anti-GFP antibody (1:1000; Roche) and mouse monoclonal anti yeast phosphoglycerate kinase (PGK1) antibody (1:5000; Invitrogen). The

secondary antibody was against mouse IgG coupled to horseradish peroxidase (HRP) (1:5000; Jackson ImmunoResearch).

The signals were revealed by chemiluminescence detection using the Immobilon Western HRP Substrate (Millipore-Merck) and a ChemiDoc XRS image system (BioRad).

III.13 Epifluorescence microscopy and flow cytometry

In the experiments using epifluorescence microscopy, cells were visualized in a Leica Microsystems DM-5000B epifluorescence microscope, with appropriate filter settings (red, green, blue and DIC (Differential Interference Contrast)) with a 100x oil immersion objective. Images were acquired with a Leica DFC350 FX Digital Camera and processed with LAS AF Microsystems software. For phenotype quantification, at least 300 cells of at least three independent experiments were evaluated.

Flow cytometry analysis was performed in an Epics[®] XLTM (BeckmanCoulter) flow cytometer equipped with an argon-ion laser emitting a 488nm beam at 15 mW. Green fluorescence emitted by SYTOX Green was collected through FL-1 sensor (505-545 nm) and red fluorescence emitted by DHE and PI was collected through FL-4 sensor (660-700 nm). For each sample 30 000 events were evaluated and data were analyzed using the FlowJo[®] 7.6 software.

III.14 Statistical Analysis

The results are presented as the mean and standard deviation (SD) values of at least three independent experiments.

Statistical analyses were performed using GraphPad Prism 6 software. P-values lower than 0.05 were assumed to represent a statistically significant difference in all experiments.

Chapter IV

Results

IV. Results

IV.1 Intracellular distribution of C9 compound

Previous studies with MSG-111-cd3 compound, using the yeast *Saccharomyces cerevisiae* as a model showed that at concentrations close to the minimum inhibitory concentration (MIC), this compound accumulates in the vacuolar membrane and in the perinuclear endoplasmic reticulum (ER) (Leitão, 2015).

To determine the intracellular distribution of C9 compound two yeast mutants were used, one expressing a GFP-tagged vacuolar membrane protein (W303-1A pDF01-VBA1-YEGFP) and other expressing a GFP-tagged ER membrane protein (BY 4741 GFP-SEC66).

Fluorescence microscopy images showed that the intracellular distribution of C9 co-localizes with the vacuolar membrane (Figure IV.1 A) and the perinuclear ER (Figure IV.1 B), indicating that C9 displays the same intracellular pattern as MSG-111-cd3 compound.

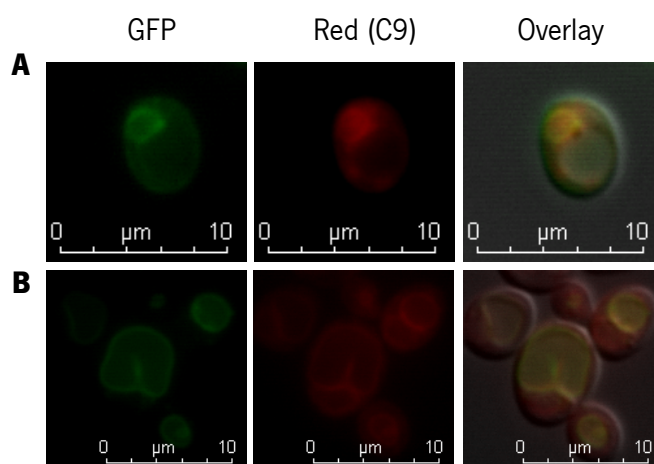


Figure IV.1 – Intracellular distribution of C9 compound – Representative fluorescence microscopy images of BY 4741 GFP-SEC66 cells treated with C9 (A). Representative fluorescence microscopy images of W303-1A pDF01-VBA1-YEGFP cells treated with C9 (B). Cells were visualized by epifluorescence microscopy with a 100x oil immersion objective.

IV.2 C9 treatment induces loss of cell viability in the yeast *Saccharomyces cerevisiae*

As described in previous studies, single differences in substituent groups of benzo[a]phenoxazines can change their antiproliferative activity (Leitão, 2015).

In order to investigate if C9 compound, as MSG-111-cd3, could induce loss of cell viability, CFU counts were measured along time of treatment with C9.

After 30 minutes of treatment a statistical significant difference between the cells treated with C9 and DMSO was observed, indicating that C9, as MSG-111-cd3, decreased the cell viability of BY 4741 cells. This effect was enhanced by the pre-treatment with the protein synthesis inhibition, cycloheximide, suggesting that *de novo* proteins synthesis may exert a protective role against the cell death-inducing activity of C9. However, the differences between cells treated with both C9 and cycloheximide and cells treated only with C9, were not statistically significant (Figure IV.2).

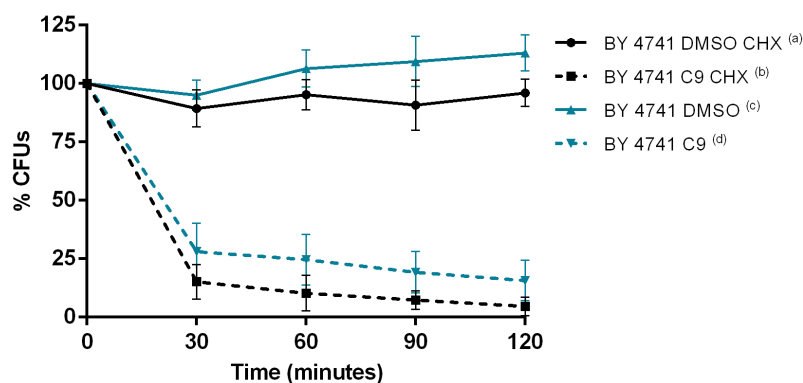


Figure IV.2 – Effect of C9 on the viability of *Saccharomyces cerevisiae* cells in the presence and absence of cycloheximide - Analysis of the inhibition of protein synthesis by cycloheximide ($100\mu\text{g ml}^{-1}$) in BY 4741 wild-type cells treated with C9 ($20\mu\text{M}$) and DMSO (0.051%). Cycloheximide and ethanol (negative control) treatment was performed 30 minutes before the C9 and DMSO incubation. Cell viability was assessed by CFU counting at different time points (0, 30, 60, 90 and 120 minutes). The reported values are means \pm SD ($n\geq 3$). Statistical analysis was performed by the two-way ANOVA test to compare cells treated with both C9 and cycloheximide, or and cells only with C9, for each time of treatment.

IV.3 Vacuolar involvement in cell death induced by C9

Vacuolar membrane permeabilization (VMP), like lysosomal membrane permeabilization (LMP) causes the release of hydrolytic enzymes from the vacuolar lumen to the cytosol which can result in cell death. The extension of VMP, partial and selective or complete disruption of the vacuole can lead to different processes and is determined by the nature of the stimulus (Boya and Kroemer, 2008; Sousa *et al.*, 2011).

As was initially demonstrated, C9 compound accumulates in vacuolar membrane. Thus, to evaluate if C9 could induce vacuolar permeabilization we used a fluorescent blue dye (CMAC) which accumulates in the lumen of vacuoles which preserve an intact membrane.

We observed that CMAC staining is localized in the vacuole lumen before treatment with C9, but after 30 minutes 25% of the cells presented a scattered blue staining pattern, reaching 70-85% after 120 minutes of treatment. In contrast, cells treated with DMSO only presented a significant

permeabilization after 120 minutes of treatment, reaching 30-40% of cells with scattered blue staining pattern (Figure IV.3). These results indicate that C9 induces a significant and progressive permeabilization of the vacuolar membrane leading to the release of their content.

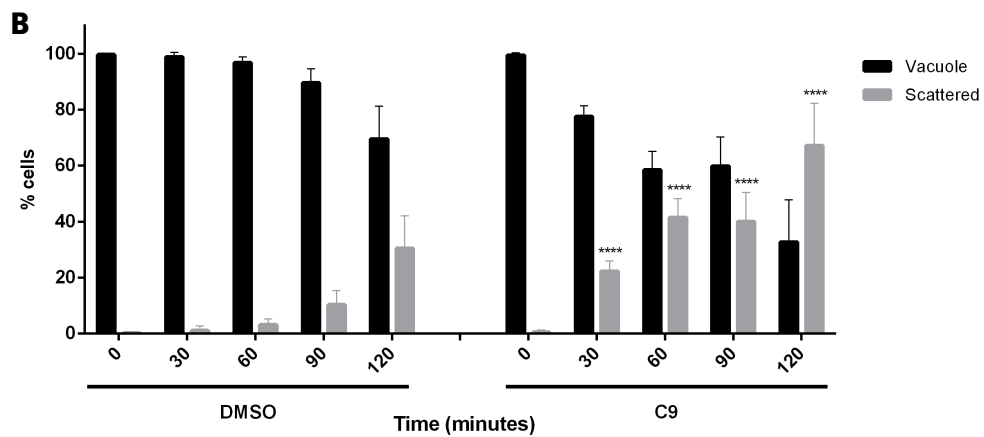
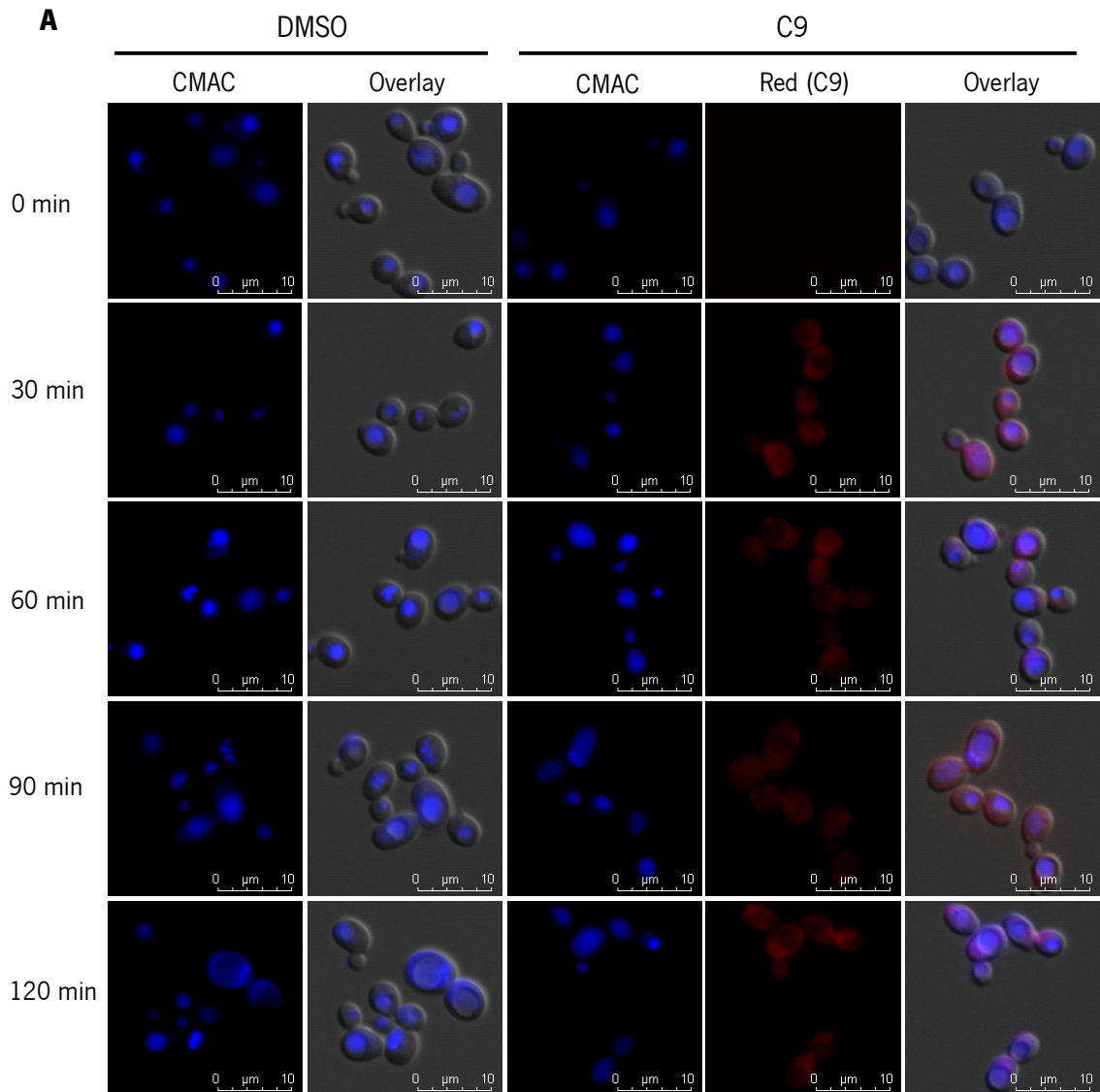


Figure IV.3 - Effect of C9 in the vacuolar membrane integrity - Fluorescence microscopy images of BY 4741 cells before (time 0) and after 30, 60, 90 and 120 minutes of treatment with C9 (7.5 μ M) and DMSO (0.038%) (negative control). Cells were stained using 2 μ M of CMAC dye and then visualized by epifluorescence microscopy with a 100x oil immersion objective **(A)**. Percentage of C9 and DMSO treated cells displaying different blue staining pattern **(B)**. At least 300 cells were counted for each condition. The reported values are means \pm SD (n \geq 5). Statistical analysis was performed by two-way ANOVA. ****P<0,0001

Yeast vacuoles are dynamic and highly regulated organelles with degradative and storage capability (Li and Kane, 2009). They are filled with several hydrolytic enzymes including proteinase A (Pep4p) ortholog of human cathepsin D, which plays an important role in apoptosis regulation (Pereira *et al.*, 2015).

Vacuolar permeabilization can lead to the release and consequent involvement of Pep4p in the cell death mechanism. In order to assess if Pep4p could be involved in C9-induced cell death, the cell viability of BY 4741 and W303-1A cells lacking Pep4p and respective wild-type strains was measured along time of treatment with this compound.

The results showed that BY 4741 $\Delta pep4$ cells displayed the same response as the wild-type cells (Figure IV.4 A). However, W303-1A $\Delta pep4$ was more sensitive when compared with wild-type cells (Figure IV.4 B). This phenotype suggests that in W303-1A background this protein plays a protective role in the mediation of the cell death process.

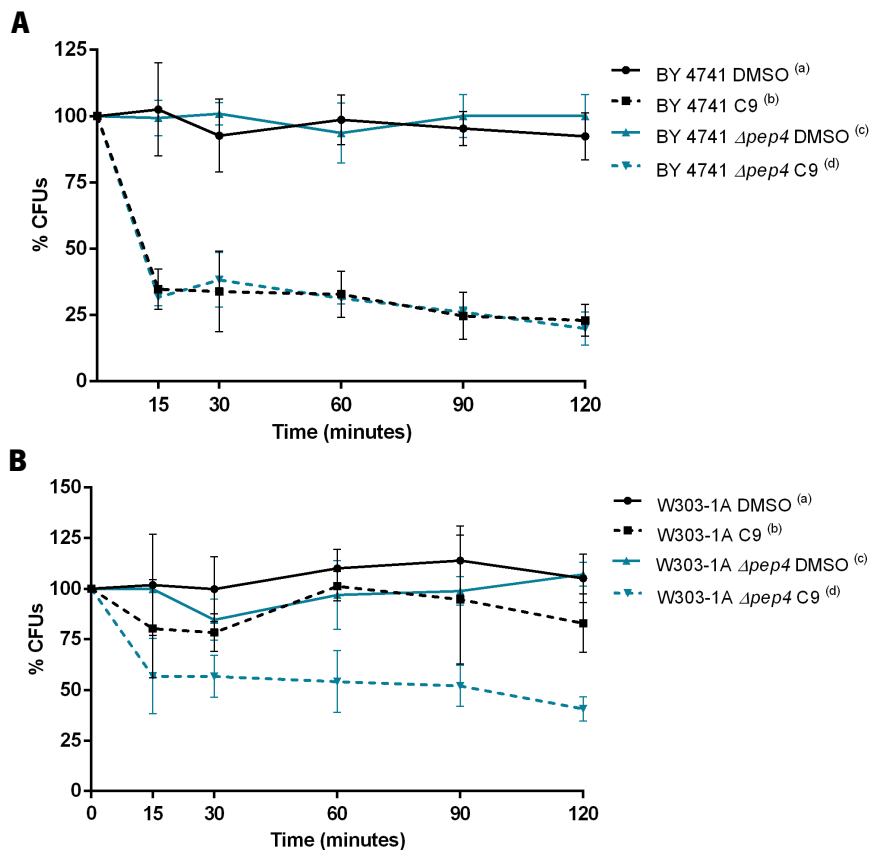


Figure IV.4 - Effect of C9 on cell viability of $\Delta pep4$ mutants - Effect of C9 (7.5 μ M) and DMSO (0.038%) (negative control) on cell viability of yeast *S. cerevisiae* BY 4741 wild-type and $\Delta pep4$ strains (A). and *S. cerevisiae* W303-1A wild-type and $\Delta pep4$ strains (B). In B) 15 min: (b vs d) ns; 30 min: (b vs d) ns; 60 min: (b vs d) **; 90 min: (b vs d) *; 120 min: (b vs d) *. Cell viability was assessed by CFU counting at different time points (0, 15, 30, 60, 90 and 120 minutes). 100% corresponds to the CFU counting before C9 and DMSO treatment. The reported values are means \pm SD (n \geq 3). Statistical analysis was performed by the two-way ANOVA. ns non-significant, *P<0.05, **P<0.01

IV.4 Mitochondrial involvement in cell death induced by C9

Beyond its crucial role in cellular energetics, mitochondria plays a central role in regulation of different scenarios acting both as a sensor of death signals and as an initiator of biochemical processes which can lead to regulated cell death (Scott and Logan, 2008; Vakifahmetoglu-Norberg *et al.*, 2017). As described in mammalian cells, lysosomal membrane permeabilization can induces cell death through mitochondria-mediated apoptosis either by caspase-dependent or – independent pathways (Sousa *et al.*, 2011).

To determine the potential mitochondrial involvement in the cell death mechanism induced by C9 treatment, cell viability assays with strains lacking several proteins described to be involved in mitochondrial-dependent cell death, such as $\Delta cpr3$ (yeast cyclophilin D), $\Delta aif1$ (yeast apoptosis inducing factor), $\Delta nuc1$ (yeast endonuclease G), $\Delta aac1/2/3$ (ADP/ATP carrier) and a strain lacking mitochondrial DNA (*rho*⁰) were performed.

No significant differences between the cell viability of BY 4741 WT, $\Delta cpr3$ and $\Delta aif1$ were observed (Figure IV.5).

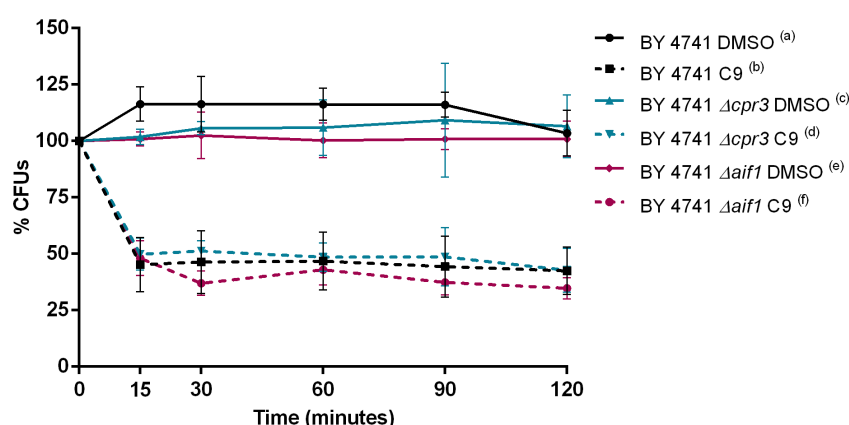


Figure IV.5 - Effect of C9 on cell viability of mitochondrial mutants - Effect of C9 (7.5 μ M) and DMSO (0.038%) (negative control) on cell viability of yeast *S. cerevisiae* BY 4741 wild-type, $\Delta cpr3$ and $\Delta aif1$ strains. Cell viability was assessed by CFU counting at different time points (0, 15, 30, 60, 90 and 120 minutes). 100% corresponds to the CFU counting before C9 and DMSO treatment. The reported values are means \pm SD (n \geq 3). Statistical analysis was performed by the two-way ANOVA.

Also, no significant difference between the cell viability of BY 4741 WT and $\Delta nuc1$ were observed (Figure IV.6 A). On the other hand, $\Delta aac1/2/3$ and rho^0 strains were more resistant when compared with respective wild-type (Figure IV.7 B, C), indicating that the absence of these proteins promotes cell survival in response to C9 treatment.

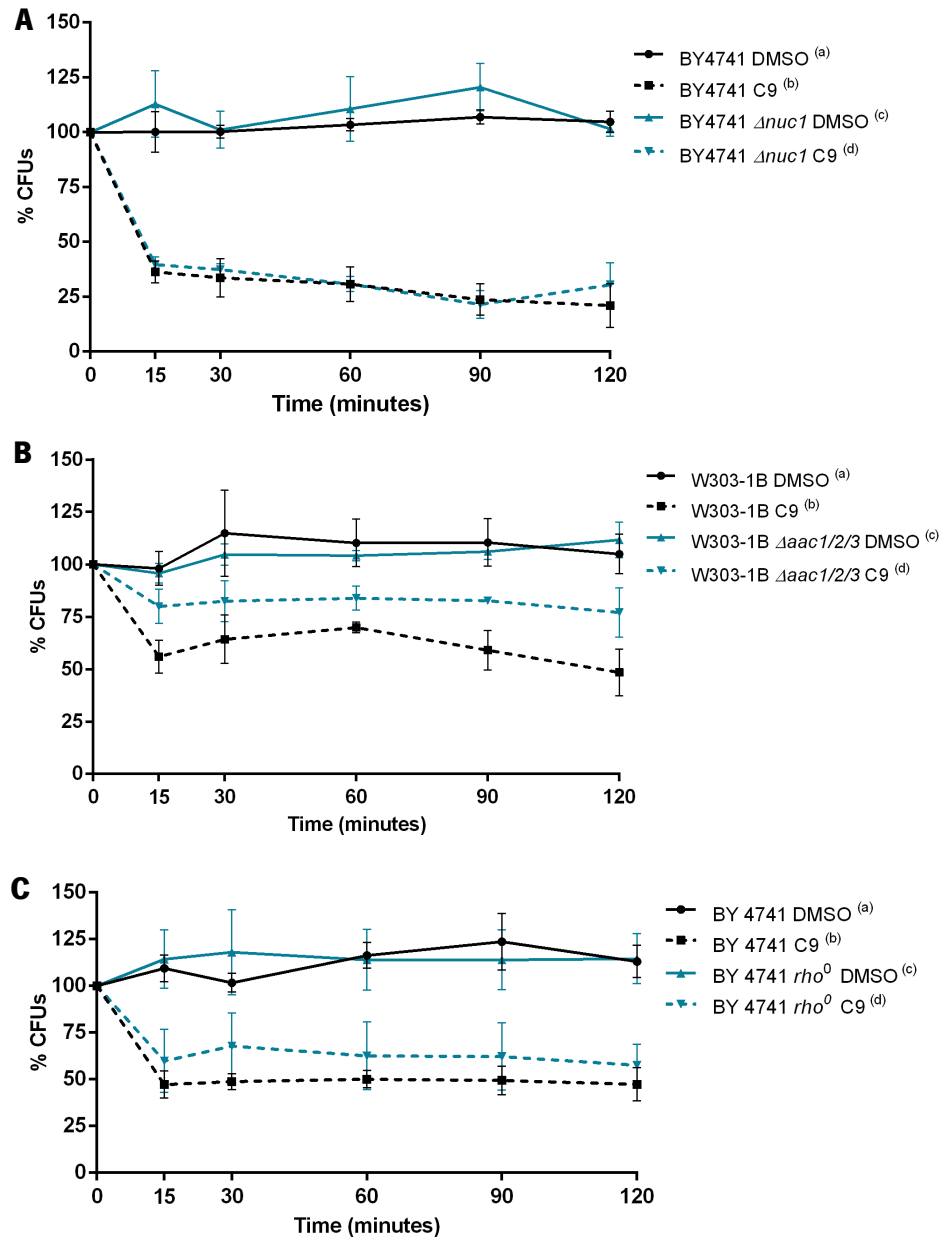


Figure IV.6 - Effect of C9 on cell viability of $\Delta nuc1$, $\Delta aac1/2/3$ and rho^0 mutants. Effect of C9 (7.5 μ M) and DMSO (0.038%) (negative control) on cell viability of yeast *S. cerevisiae* BY 4741 wild-type and $\Delta nuc1$ strains (A), and yeast *S. cerevisiae* W303-1B wild-type and $\Delta aac1/2/3$ strains (B) and *S. cerevisiae* BY 4741 wild-type and rho^0 strains (C). In B 15 min: (b vs d)**; 90 min: (b vs d)**; 120 min: (b vs d)** . In C 30 min (b vs d)*. Cell viability was assessed by CFU counting at different time points (0, 15, 30, 60, 90 and 120 minutes). 100% corresponds to the CFU counting before C9 and DMSO treatment. The reported values are means \pm SD (n \geq 3). Statistical analysis was performed by the two-way ANOVA. *P<0.05, **P<0.01, ***P<0.001

Mitochondria are also dynamic organelles that constantly fuse and divide, changing from interconnected networks to multiple fragmented mitochondria, providing an efficient adaptation to the cell metabolic needs. These changes in mitochondrial morphology are often associated with early events of yeast regulated cell death (Braun and Westermann, 2011).

In order to assess if C9 treatment leads to mitochondrial network fragmentation, W303-1A cells transformed with pYX-mt-GFP, which encode a mitochondrial-addressed GFP, were visualized by epifluorescence microscopy along 120 minutes of treatment.

As expected, cells treated with DMSO (negative control) presented defined interconnected networks. However, after 30 minutes of C9 treatment, mitochondrial networks were fragmented, leading to the formation of punctuated structures (Figure IV.7).

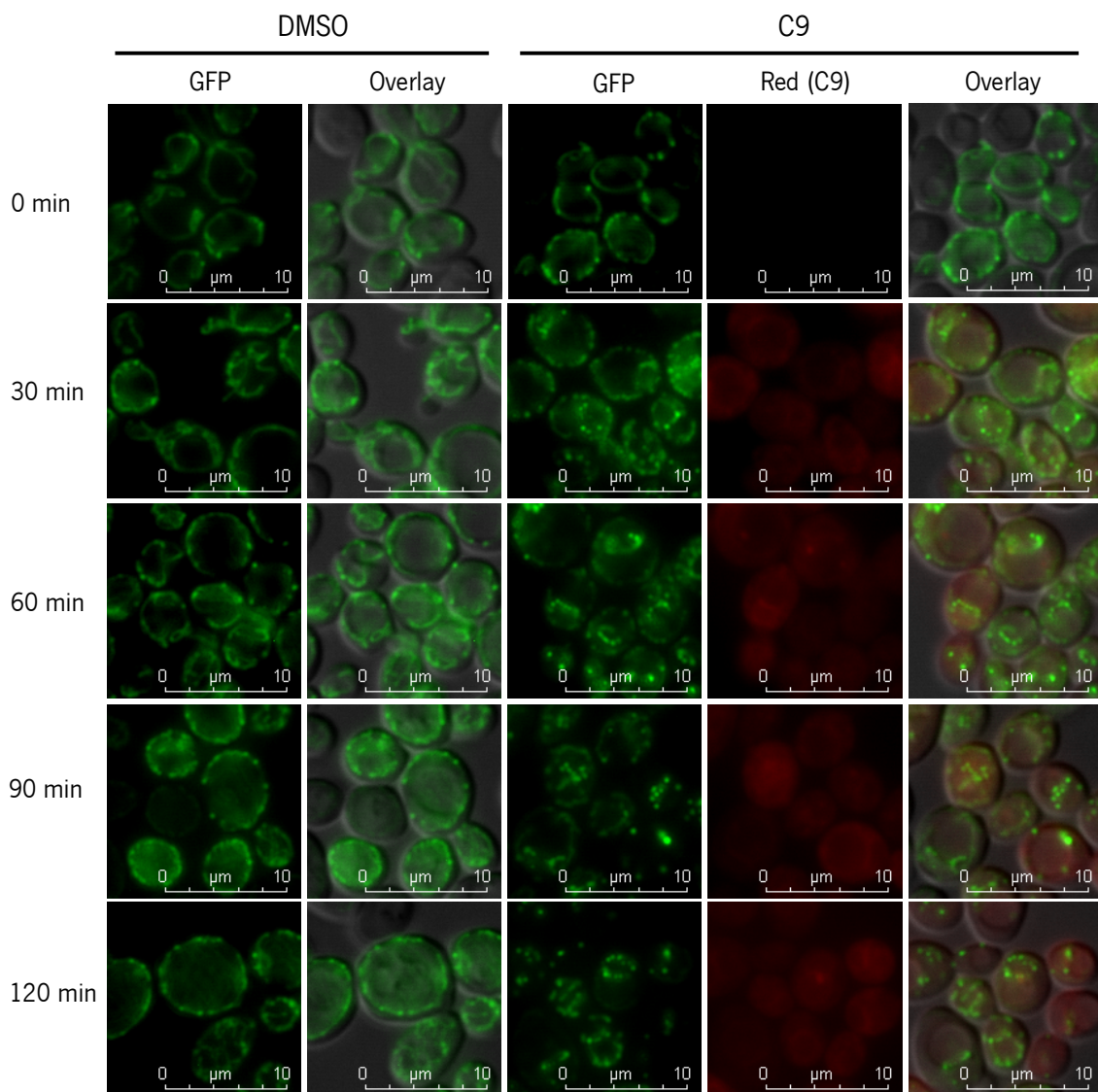


Figure IV.7 - Effect of C9 on mitochondrial network - Fluorescence microscopy images of W303-1A pYX-mt-GFP cells before (time 0) and after 30, 60, 90 and 120 minutes of treatment with C9 (7.5 μ M) and DMSO (0.038%) (negative control). Cells were visualized by epifluorescence microscopy with a 100x oil immersion objective.

IV.5 Metacaspase involvement in cell death induced by C9

As described for mammalian caspases, also yeast metacaspase is involved in the regulation of cell death process. Studies demonstrated that in response to H_2O_2 , Yca1p is implied in the process of apoptotic mitochondrial fragmentation (Mazzoni and Falcone, 2008). So, to evaluate the metacaspase involvement in the cell death induced by C9 treatment, cell viability assays with a strain lacking yeast metacaspase (Yca1p) were performed.

The results demonstrate that $\Delta yca1$ cells were significantly more resistant when compared with WT cells, suggesting that Yca1p displays an effector role in mediation of C9-induced cell death (Figure IV.8).

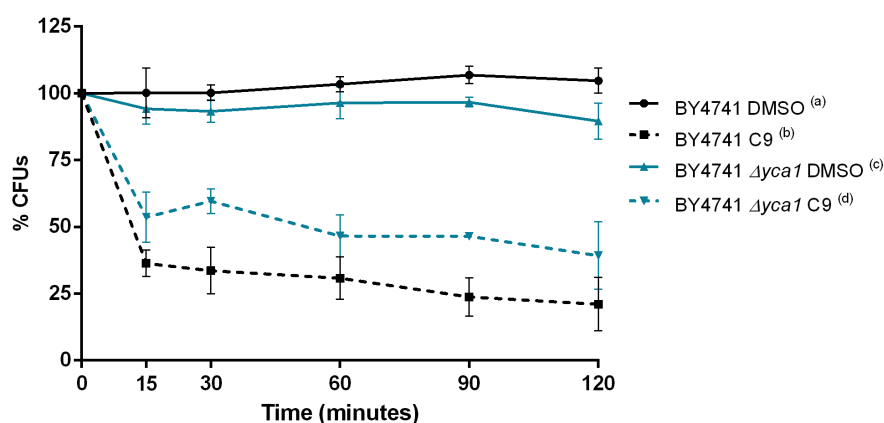


Figure IV.8 - Effect of C9 on cell viability of $\Delta yca1$ mutant. Effect of C9 (7.5 μ M) and DMSO (0.038%) (negative control) on cell viability of yeast BY 4741 wild-type and $\Delta yca1$ strains. 15 min: (b vs d) **; 30 min: (b vs d) ***; 60 min: (b vs d) *; 90 min: (b vs d) ***; 120 min: (b vs d) **. Cell viability was assessed by CFU counting at different time points (0, 15, 30, 60, 90 and 120 minutes). 100% corresponds to the CFU counting before C9 and DMSO treatment. The reported values are means \pm SD ($n \geq 3$). Statistical analysis was performed by the two-way ANOVA. * $P < 0.05$, ** $P < 0.01$, *** $P < 0.001$

IV.6 Assessment of the accumulation of reactive oxygen species

When cell antioxidant defenses fail to impede ROS accumulation, the oxidative damage of cell biomolecules like proteins, lipids, DNA and consequent damage of specific organelles such as mitochondria and lysosome (Blomgran *et al.*, 2007), can compromise cell homeostatic functions and cell viability leading to cell death (Farrugia and Balzan, 2012).

To assess if C9 treatment leads to ROS accumulation and consequent oxidative damage, BY 4741 cells collect at indicated time points before and after treatment were stained with DHE, a specific probe for monitoring intracellular superoxide anion, and analyzed by flow cytometry. As a positive control for DHE staining treatment with hydrogen peroxide (H_2O_2) was used.

The results indicate that there are significant differences between cells treated with C9 and treated with DMSO after 90 minutes, although, the percentages of cells displaying ROS accumulation is not enough to justify the high loss of cell viability induced by C9 treatment (Figure IV.9).

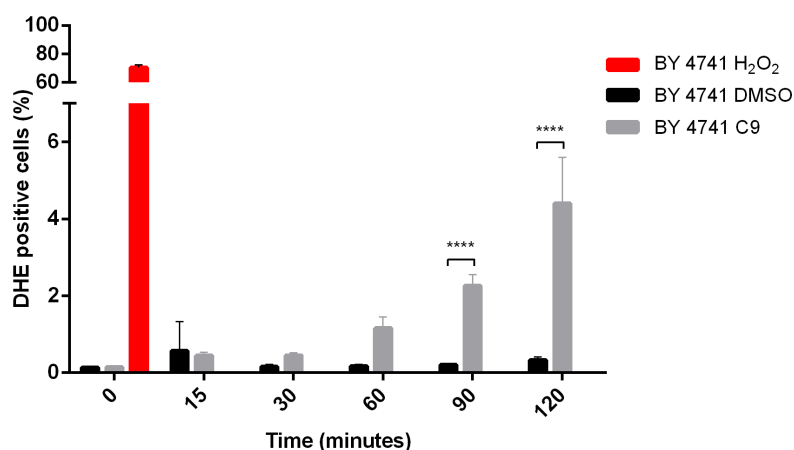


Figure IV.9 – Analysis of reactive oxygen species (ROS) accumulation in response to C9 treatment - Effect of C9 and DMSO (negative control) on ROS accumulation of BY 4741 wild-type cells. Yeast cells were treated with C9 (7.5 μ M) and DMSO (0.038%). As a positive control for DHE staining cells treated with hydrogen peroxide (H₂O₂) were used. For flow cytometry analysis, the cells were collected at different time points before (time 0) and after 15, 30, 60, 90 and 120 minutes of treatment and then stained with 2 μ g ml⁻¹ of DHE. Results are expressed as percentage of DHE positive population. The reported values are means with SD (n \geq 3). Statistical analysis was performed by the two-way ANOVA. ****P<0,0001

IV.6 Autophagy involvement in cell death induced by C9

As previously described, autophagy maintains the organism homeostasis through its involvement in various cellular processes including the degradation of aberrant structures and turnover of superfluous or dysfunctional organelles like mitochondria (mitophagy), which increases the cell survival, as well as the involvement in cell growth, development and cell death (Boya *et al.*, 2013; Chen and Klionsky, 2011).

Thus, to determine if the autophagic machinery is involved in the cell death mechanism induced by C9 treatment. For that, cell viability assays with strains lacking proteins that are involved in the autophagic process, such as Atg1p (essential protein for the initiation of autophagy), Atg5p (protein involved in the phagophore expansion) and Atg32p (mitochondrial outer membrane protein that is required for mitophagy) were performed.

The results demonstrate that no significant differences between the cell viability of wild-type and Δ atg1 strains were observed (Figure IV.10 A). However, Δ atg5 strain is more sensitive when

compared with wild-type strain, indicating that Atg5p is involved in the mediation of the cell death process induced by C9 treatment. Also, $\Delta atg32$ strain seems to be more sensitive after 60 minutes of treatment although this difference is not statistically significant (Figure IV.10 B).

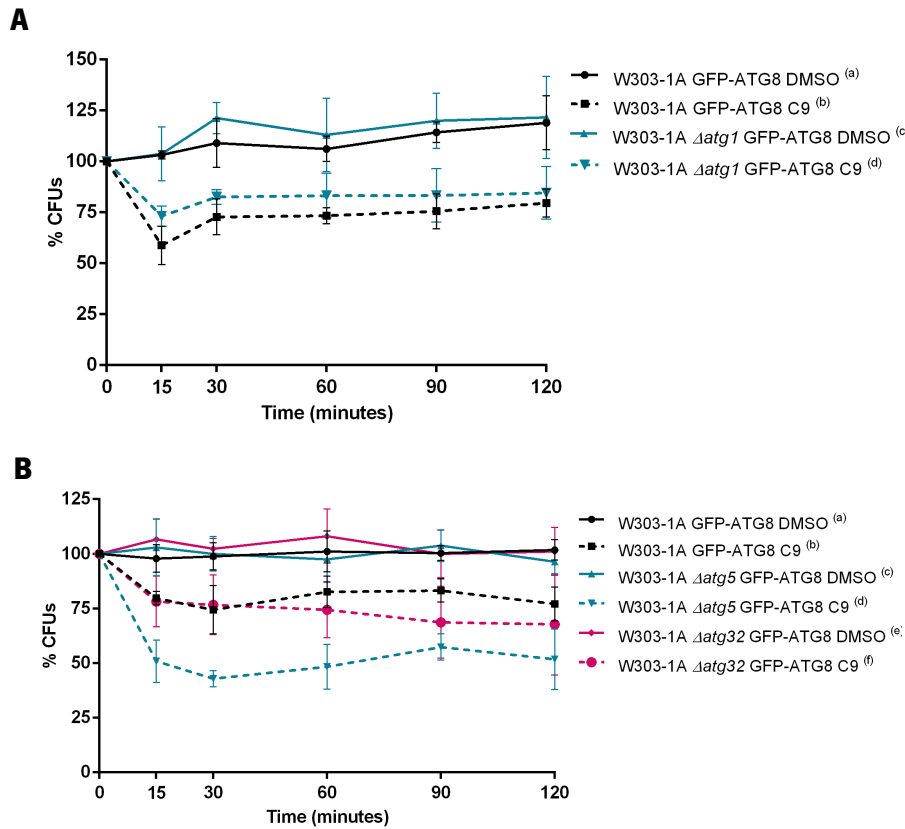


Figure IV.10 - Effect of C9 on cell viability of autophagic mutants – Effect of C9 (7.5 μ M) and DMSO (0.038%) (negative control) on cell viability of yeast *S. cerevisiae* W303-1A wild-type and $\Delta atg1$ strains (**A**), and yeast *S. cerevisiae* W303-1A wild-type, $\Delta atg5$ and $\Delta atg32$ strains (**B**). In **B** 15 min: (b vs d) ***, (d vs f) **, 30 min: (b vs d) ***, (d vs f) ****, 60 min: (b vs d) ****, (d vs f) **, 90 min: (b vs d) **, 120 min: (b vs d) **. The percentage of cell viability was assessed by CFU counting at different time points (0, 15, 30, 60, 90 and 120 minutes). 100% corresponds to the CFU counting before C9 and DMSO treatment. The reported values are means \pm SD (n \geq 3). Statistical analysis was performed by the two-way ANOVA. **P<0.01, ***P<0.001, ****P<0.0001

In addition to viability assays, we also assessed the autophagic flux and its degradation activity, by performing GFP-Atg8 monitoring assays. When autophagy is active, the GFP-Atg8 fusion protein is incorporated into autophagosome and delivery to the vacuole, where it is degraded by vacuolar hydrolases leading to the accumulation of free GFP (Carmona-Gutierrez *et al.*, 2018; Torggler *et al.*, 2017). Breakdown of GFP-Atg8 fusion protein allows the measurement of the autophagic rate (Chen and Klionsky, 2011). So, W303-1A GFP-ATG8, $\Delta atg1$ GFP-ATG8, $\Delta atg5$ GFP-ATG8 and $\Delta atg32$ GFP-ATG8 strains treated with treated with C9 and DMSO, and also with rapamycin (RP)

as a positive control for autophagy induction, were collected at specific time points for epifluorescence microscopy observation and western blot analysis.

Fluorescence microscopy images showed green fluorescence in the vacuole lumen after 60 minutes of DMSO and RP treatment in WT cells, as well as in $\Delta atg32$ cells treated with RP (Figure IV.11 A). On the other hand, scattered green fluorescence can be visualized in the cytosol of $\Delta atg1$ and $\Delta atg5$ cells treated with DMSO and RP (Figure IV.11 B).

Autophagy induction was confirmed by western blot analysis, where the appearance of cleaved GFP band was observed in WT and $\Delta atg32$ cells treated with DMSO and RP, being these bands less visible in $\Delta atg32$ cells (Figure IV.12). The confirmation of blocked autophagy in $\Delta atg1$ and $\Delta atg5$ cells was confirmed by the absence of cleaved GFP band in all conditions.

Fluorescence microscopy images also showed that after 60 minutes of treatment with C9, green fluorescence was not observed only in the vacuole lumen of WT cells, instead, the C9 treatment leads to a scattered green fluorescence pattern in the cytosol or the overall cell (Figure 16A). In addition, $\Delta atg1$, $\Delta atg5$ and $\Delta atg32$ cells only demonstrate scattered green fluorescence in the cytosol (Figure IV.11 A, B).

The previous results were confirmed by western blot analysis, where in WT cells the appearance of a less visible cleaved GFP band was observed upon treatment with C9 when compared to cells treated with DMSO and RP, suggesting that C9 blocks autophagy induction (Figure IV.12). Because the assays were carried out in PBS 1x, possibly leading to nutrient starvation, autophagy induction in WT cells treated with C9 and DMSO may have been due to starvation and not DMSO treatment, in any case C9 seems to decrease autophagy induction.

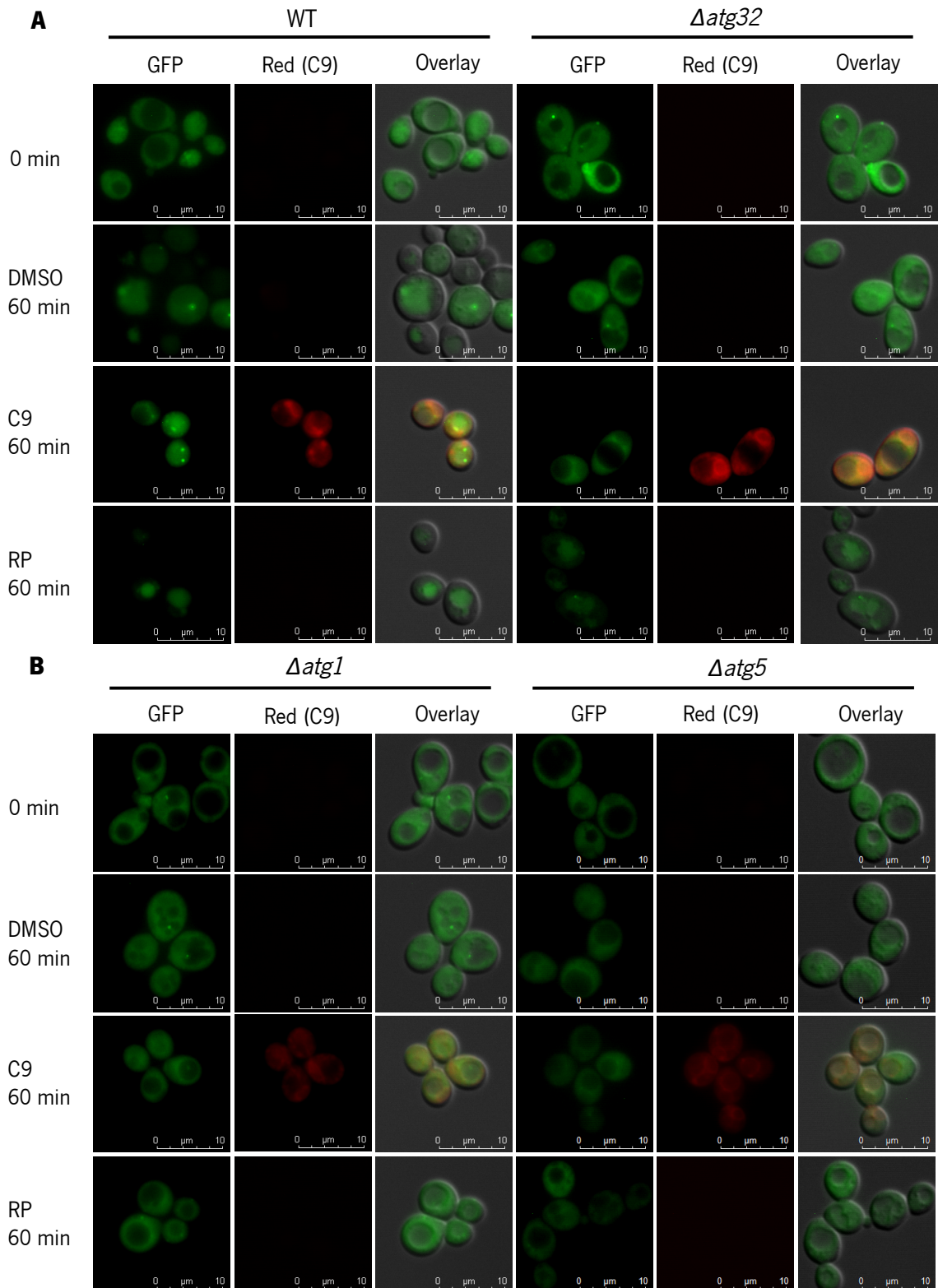


Figure IV.11 - Analysis of Atg8p localization in response to C9 treatment – Fluorescence microscopy images of W303-1A GFP-ATG8 and *Δatg32* GFP-ATG8 cells, before and after 60 minutes of treatment with C9, DMSO and RP (**A**). Fluorescence microscopy images of W303-1A *Δatg5* GFP-ATG8 and *Δatg32* GFP-ATG8 cells, before and after 60 minutes of treatment with C9, DMSO and RP (**B**). Cells were treated with 7.5 μM of C9, 0.038% of DMSO (negative control) and 0.2 $\mu\text{g ml}^{-1}$ of Rapamycin (RP-positive control), collected before (time 0) and after 60 minutes of treatment and then visualized by epifluorescence microscopy with a 100x oil immersion objective.

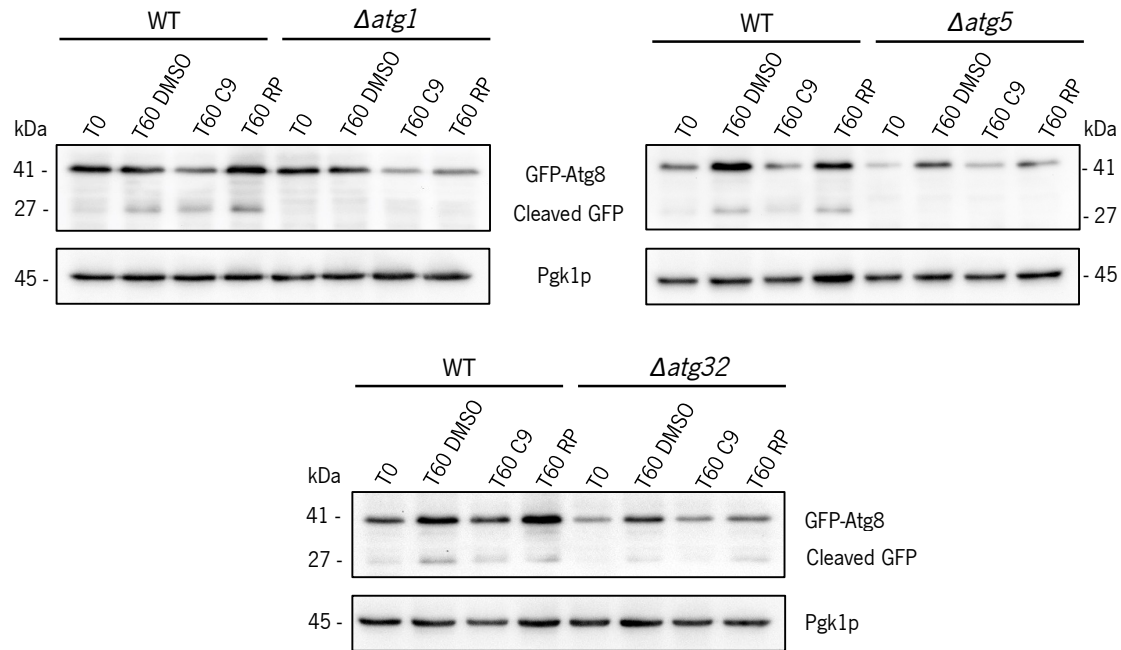


Figure IV.12 – Western blot analysis of GFP-Atg8 processing – Effect of C9, DMSO (negative control) and Rapamycin (RP-positive control) on GFP-Atg8 processing. Protein extracts were obtained from W303-1A GFP-ATG8, $\Delta atg1$ GFP-ATG8, $\Delta atg5$ GFP-ATG8 and $\Delta atg32$ GFP-ATG8 cells collected before (time 0) and after 60 minutes of treatment with 7.5 μ M of C9, 0.038% of DMSO and 0.2 μ g ml⁻¹ of Rapamycin. Pgk1p was used as a loading control.

IV.7 Assessment of nuclear changes induced by C9 treatment

In apoptotic cell death, cells are characterized by several morphological alteration like DNA fragmentation, represented by appearance of DNA strand breaks and diminished DNA content (sub-G0/G1), chromatin condensation (pyknosis) and nuclear fragmentation (karyorrhexis) (Azzopardi *et al.*, 2017; Plesca *et al.*, 2008).

To assess the cell cycle distribution and consequently the detection of sub-G0/G1 population, cell cycle analysis by flow cytometry was performed.

No significant differences between the number of cells in sub-G0/G1 phase of cells treated with C9 and DMSO were observed (Figure IV.13). Also, there is no major progression in cell cycle consistent with the absence of cell proliferation, but a slight increase in G0/G1 is observed.

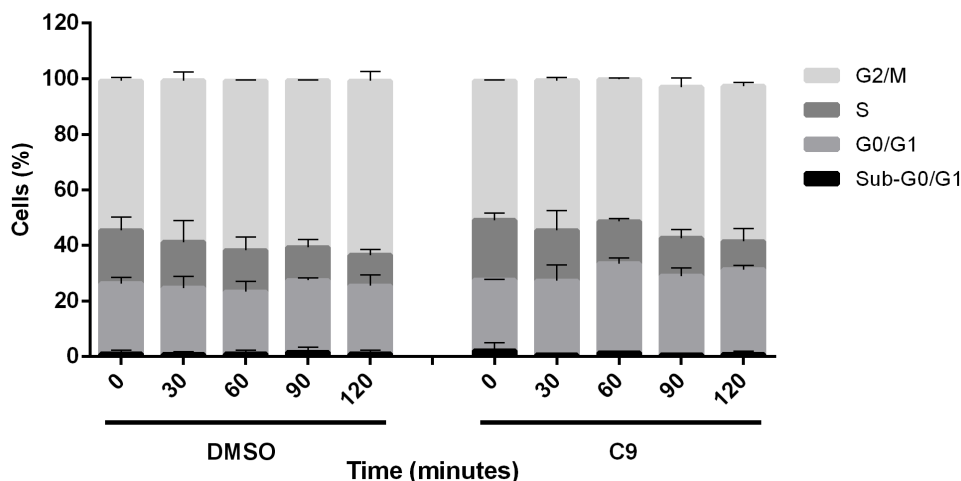


Figure IV.13 – Cell cycle analysis in response to C9 treatment - Effect of C9 and DMSO (negative control) on cell cycle progression of BY 4741 wild-type cells. Yeast cells were treated with C9 (7.5 μ M) and DMSO (0.038%). For flow cytometry analysis, the cells were collected at different time points before (time 0) and after 30, 60, 90 and 120 minutes of treatment and then stained with 1 μ M of SYTOX Green. Results are expressed as percentage of cells in each cell cycle phase. The reported values are means with SD ($n \geq 2$). Statistical analysis was performed by the two-way ANOVA.

IV.8 Assessment of plasma membrane integrity

As a clear death phenotype was not found, to assess if the cell death induced by C9 could be necrotic or apoptotic, next plasma membrane integrity was determined. For such cells were stained with exclusion dye propidium iodide (PI). PI is an intercalating agent that can bind to nucleic acids of dead cells or cells with damaged membrane, and is blocked by viable cells with intact membrane (Gutierrez *et al.*, 2018; Kwolek-Mirek and Zadrąg-Tecza, 2014).

BY 4741 cells collect at indicated time points before and after C9 and DMSO treatment were stained with PI and analyzed by flow cytometry. As a positive control for PI staining boiled cells were used.

PI positive cells did not increase significantly, reaching only 1.5% after 120 minutes of treatment with C9 (Figure IV.14). No significant differences between DMSO and C9 were observed, indicating that this compound does not lead to loss of plasma membrane integrity.

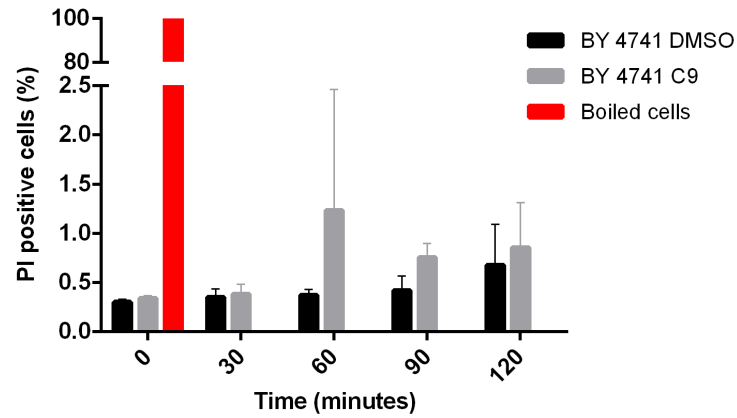


Figure IV.14 – Analysis of plasma membrane integrity in response to C9 - Effect of C9 and DMSO (negative control) on plasma membrane integrity of BY 4741 wild-type cells stained with propidium iodide (PI). Yeast cells were treated with C9 (7.5 μ M) and DMSO (0.038%). Boiled cells are used as a positive control for PI staining. For flow cytometry analysis the cells were collected at different time points before (time 0) and after 15, 30, 60, 90 and 120 minutes of treatment and then stained with 2 μ g ml⁻¹ of PI. Results are expressed as percentage of PI positive population. The reported values are means with SD (n \geq 3). Statistical analysis was performed by the two-way ANOVA.

Chapter V

Discussion and Future perspectives

V. Discussion and Future perspectives

Phenoxazine derivatives are versatile compounds that can be used as fluorescent dyes as well as antiproliferative agents. These potentialities have led our group to synthesize new benzo[*a*]phenoxazine compounds that have been shown to have an interesting potential as antifungal agents (Frade *et al.*, 2008). Based on these results several studies have been conducted to elucidate the mechanisms underlying the effect of one specific compound, the MSG-111cd3, that showed high antifungal activity (Frade *et al.*, 2007; Carvalho, 2011). It was observed that this compound induces a regulated cell death process which may be mediated through the permeabilization of the vacuolar membrane, without the involvement of autophagy and mitochondrial pathways (Ferreira, 2017; Lopes, 2015). Thus, in order to continue the study of those benzo[*a*]phenoxazine activities and also to relate the structure with the activity, in this work C9 compound that differs from MSG-111-cd3 only in a single substitution of its extended aromatic system which increases its antifungal activity was used.

Our results demonstrate that similarly to MSG-111-cd3 also C9 compound accumulates at the vacuolar membrane and the perinuclear endoplasmic reticulum. These results indicate that the intracellular distribution is not affected by the structural differences between the two compounds. The yeast ER is involved in the execution of many cellular functions including protein synthesis and translocation, lipid synthesis and calcium homeostasis (Austriaco, 2012). The disruption of ER function leads to ER stress which can induce cell death (Austriaco, 2012; Falcone and Mazzoni, 2016; Kim *et al.*, 2009). As such, in the future it is important to assess if C9 activity can induce yeast ER stress or other alterations in ER functions and components.

In agreement with its accumulation at the vacuolar membrane, C9 leads to vacuolar permeabilization assessed through CMAC staining. In fact, after 120 minutes of treatment, 70-85% of the cells evidence a scattered blue staining pattern due to CMAC release from vacuolar lumen. As described in the literature, the magnitude of the lysosomal and vacuolar permeabilization and consequent amount of released hydrolases from the lysosome to the cytosol can determine different subroutines of cell death (Guicciardi *et al.*, 2004; Sousa *et al.*, 2011). In other words, massive rupture of the lysosome triggers uncontrolled release of lysosomal content which can induce a cell death by necrosis. In contrast, partial and selective lysosomal permeabilization induce a controlled hydrolysis which can promote a cell death by apoptosis-like cell death (Kirkegaard and Jäättelä, 2009; Serrano-Puebla and Boya, 2016). Therefore, it would be interesting the determination of the vacuole morphology, namely if C9 induces vacuolar fragmentation to assess

the extent of vacuolar damage. Nevertheless, the results from PI staining assays showed that the plasma membrane retains its integrity, even at the end of the 120 min. treatment, arguing against the occurrence of a necrotic process.

It is accepted that the vacuolar hydrolases as Pep4p, yeast orthologs of mammalian cathepsin D, are involved in the regulation of cell death (Sousa *et al.*, 2011). In this work, we observed that in BY 4741 cells Pep4p does not seem to have a role in cell death. However, in W303-1A background Pep4p seems to play a protective role in the mediation of cell death process induced by C9 treatment. The same phenotype was observed in acetic acid treatment, where cells lacking Pep4p displayed higher vulnerability, while cells overexpressing Pep4p demonstrated higher resistance (Pereira *et al.*, 2010). On the other hand, in MSG-111-cd3 induced cell death this protein has an effector role (Ferreira, 2017). These findings suggest that the Pep4p can have either an effector or protective role depending on the cell death stimuli. Further studies it will be necessary to confirm the BY 4741 phenotype as well as Pep4p release from the vacuole.

We also studied the mitochondrial involvement underlying C9 toxicity. Beyond their major function as powerhouse of the cell, mitochondria also play a fundamental role in the regulation of several signals which can determinate different cellular outcomes as proliferation, adaptation to environmental changes and cell death (Vakifahmetoglu-Norberg *et al.*, 2017). The crucial feature in mitochondria-mediated cell death is the mitochondrial outer membrane permeabilization (MOMP) which can promote the release of apoptogenic factors as cytochrome *c* (cyt *c*), apoptosis inducing factor (AIF) and endonuclease G (Falcone and Mazzoni, 2016; Pereira *et al.*, 2008). In our work, we observed that Aif1p (apoptosis inducing factor) and Nuc1p (yeast endonuclease G) proteins are not involved in the regulation of this cell death process. The three ADP/ATP carrier isoforms (Aac1/2/3) and the mitochondrial cyclophilin D (Cpr3p) that are components of the mitochondrial permeability transition pore (PTP), which can mediate MOMP, were also evaluated, showing that unlike Cpr3p, Aac1/2/3p are involved and play an effector role in the C9-induced cell death mechanism. This phenotype was observed in acetic acid and diamide treatment where the absence of AAC proteins protects the cells (Pereira *et al.*, 2007). However, it is important to access if this phenotype could be due to the direct involvement of AAC proteins or could result from oxidative phosphorylation deficiency which decreases the respiration rates and ATP levels.

The execution of mitochondrial functions in response to cell metabolic needs is directly dependent on the maintenance of tubular structures in an equilibrium between fission and fusion events (Braun and Westermann, 2011; Falcone and Mazzoni, 2016). The disruption of this

equilibrium which promotes mitochondrial fragmentation can be associated with cell death processes induced by several antifungal agents including amiodarone, H₂O₂, ethanol and acetic acid (Cheng *et al.*, 2008). Our data clearly demonstrate that C9 activity induces alterations in mitochondrial morphology, changing from interconnected networks to punctuated structures consistent with mitochondrial fragmentation which occurs only after 30 minutes of treatment. Specific proteins including Dnm1p, Mdv1p and Fis1p are involved in the regulation of mitochondrial fission in healthy cells (Cheng *et al.*, 2008). However, it is reported that the deletion of these proteins increase the cell resistance against different cell death stimuli (Braun and Westermann, 2011; Fannjiang *et al.*, 2004). As such, it is important to evaluate if the cell survival in response to C9 treatment can be increased by the inhibition or the increase of mitochondrial fusion.

In addition, the phenotype observed in *rho^o* cells, where the lack of mitochondrial DNA increases the cell survival to C9 treatment, can further indicate the mitochondrial involvement in the cell death mechanism induced by C9. However, the mechanism underlying mitochondrial involvement is still unclear, so it will be necessary identify other markers such as the release of cytochrome *c*, alterations in mitochondrial membrane potential as well as alterations in calcium (Ca²⁺) homeostasis which also mediates the initiation and execution of cell death (Pinton *et al.*, 2008).

In mammalian cells, the caspase activation has been described as one of the key processes in apoptosis. As caspases, also yeast metacaspase (Yca1p) is involved in the regulation of the cell death. Our results demonstrate that the deletion of Yca1p increases the cell survival when the cells were treated with C9, suggesting that this protein displays an effector role in the C9-induced cell death. The same phenotype was described in cells treated with H₂O₂ where the deletion of Yca1p disrupted the apoptotic machinery, increasing the cell survival, and the overexpression enhanced cell death (Mazzoni and Falcone, 2008). Moreover, Yca1p also has been implied in the process of apoptotic mitochondrial fragmentation in response to the same stimulus (Pereira *et al.*, 2008). These evidences raise the hypothesis of the involvement of Yca1p in the mitochondrial fragmentation observed in C9 treatment. For addressing this hypothesis will be necessary assess the activation of yeast metacaspase and mitochondrial fragmentation in an Yca1p deficient strain. On the other hand, it has been estimated that only 40% of the described yeast cell death process are dependent of Yca1p (Falcone and Mazzoni, 2016), indicating that other pathways may be involved such as the permeabilization of vacuolar membrane and action of cathepsins (Sousa *et al.*, 2011).

Another common feature in the regulated cell death processes is the accumulation of ROS. In physiological concentrations ROS participates in signal transduction events associated with cell vital functions, while in excessive concentrations they overcome the antioxidant defenses inducing oxidative damage of the cell biomolecules which can lead to cell death (Blomgran *et al.*, 2007; Simon *et al.*, 2000). Oxidative stress is also described to be involved in the damage of specific organelles such as mitochondrial and lysosome, promoting the faster and direct effect on the permeabilization of the vacuolar membrane (Blomgran *et al.*, 2007). However, the existence of mitochondrial and vacuolar stress as well as the decrease in cell viability induced by C9 treatment does not seem to involve ROS because, although the ROS accumulation increased along treatment, only 6% of cells displayed this increase after 120 minutes of treatment with C9.

As autophagy is a stress-induced catabolic process that is involved in several physiological processes including the adaptation to starvation, the degradation of aberrant structures and life extension, but also cell death when overstimulated (Boya *et al.*, 2013; Chen and Klionsky, 2011), we evaluate its involvement in C9-induced cell death. We are able to observe that C9 treatment seems to inhibit the autophagy induction which can be a consequence of vacuolar permeabilization (Serrano-Puebla and Boya, 2016). However, the cell viability assays demonstrated that cells lacking Atg5p presented a decreased cell viability, in opposition to the cells lacking the Atg1p and Atg32p that do not seem to be involved in this cell death process. Atg5p is covalently linked to Atg12p, generating the Atg12-Atg5 complex involved in the phagophore expansion (Boya *et al.*, 2013), thus it will be interesting to assess if the same phenotype is observed in cells lacking Atg12p, indicating that this step of the autophagic mechanism is involved in resistance to C9 activity or if only Atg5p is involved. Furthermore, recent studies in pancreatic acinar cells demonstrate that the knockout of Atg5p or Atg7p promotes ER dilation and stress which can lead to cell death (Smith and Wilkinson, 2017). These findings further suggest the ER involvement in the cell death mechanism induced by C9 and are in agreement with the observed C9 accumulation at this organelle.

Beside the above described apoptotic markers, we also assess the appearance of sub-G0/G1 population which is characterized by a diminished DNA content. However, the C9 treatment does not seem to increase sub-G0/G1 population that is characteristic of an apoptotic cell death.

Benzophenoxazine derivatives can exert their antiproliferative activity, by the interaction with DNA, intercalating between the base pairs through hydrogen bonds and π - π stacking interactions leading to the disruption of the normal DNA function (Bolognese *et al.*, 2002a; Bolognese *et al.*,

2002b). Thus, in the future it will be important to assess if C9 activity can induce other nuclear changes such as DNA fragmentation, as well as chromatin condensation.

Finally, since we could not find either a clear apoptotic or necrotic phenotype, we assess the plasma membrane integrity by PI exclusion which revealed a lower percentage of PI positive cells reaching only 1.5% after 120 minutes of treatment with C9, suggesting that a necrotic cell death does not seem to be induced. However, it has been reported that cells treated with palmitoleic acid (POA) can undergo a subtype of necrotic cell death, the liponecrosis, without the rupture of the plasma membrane (Falcone and Mazzoni, 2016), but this mechanism is different from that induced by C9.

In summary, we show that C9 induces cell death in *S. cerevisiae*, accompanied by vacuolar membrane permeabilization and consequent involvement of Pep4p. In fact, the absence of Pep4p decreases the cell survival in response to C9 treatment, suggesting that this protein plays a protective role in the cell death process. The mediation of cell death, apparently, involves the yeast metacaspase Yca1p, since deficiency in this protein leads to higher resistance. Besides vacuole, also mitochondria seem to be implicated in C9-induced cell death. The resistance phenotype observed in cells lacking AAC proteins and mitochondrial DNA is in agreement with mitochondrial involvement. Which undergo extensive fragmentation as consequence of C9 treatment. Furthermore, C9 does not seem to induce a necrotic cell death because no loss of plasma membrane integrity was observed. Although the autophagy does not seem to be involved, the deletion of Atg5p decrease the cell survival, indicating that this protein displayed a protective role. As a whole, the results point to the occurrence of a regulated cell death process mediated by the vacuolar permeabilization and mitochondrial involvement.

This work provides new insights for the use of benzo[*a*]phenoxazine as antifungal agents, characterizing their activity in order to evaluate their potential application.

Chapter VI

References

VI. References

- Alberti, A., Bolognese, A., Guerra, M., Lavecchia, A., Macciantelli, D., Marcaccio, M., ... Paolucci, F. (2003). Antitumor Agents 4. Characterization of Free Radicals Produced during Reduction of the Antitumor Drug 5H-Pyridophenoxazin-5-one: An EPR Study. *Biochemistry*, *42*(41), 11924–11931. <http://doi.org/10.1021/bi0346087>
- Allocati, N., Masulli, M., Di Ilio, C., and De Laurenzi, V. (2015). Die for the community: An overview of programmed cell death in bacteria. *Cell Death and Disease*, *6*(1), e1609-10. <http://doi.org/10.1038/cddis.2014.570>
- Austriaco, O. P., N. (2012). Endoplasmic reticulum involvement in yeast cell death. *Frontiers in Oncology*, *2*(August), 1–6. <http://doi.org/10.3389/fonc.2012.00087>
- Azzopardi, M., Farrugia, G., and Balzan, R. (2017). Cell-cycle involvement in autophagy and apoptosis in yeast. *Mechanisms of Ageing and Development*, *161*, 211–224. <http://doi.org/10.1016/j.mad.2016.07.006>
- Baehrecke, E. H. (2002). How death shapes life during development. *Nature Reviews Molecular Cell Biology*, *3*(10), 779–787. <http://doi.org/10.1038/nrm931>
- Blomgran, R., Zheng, L., and Stendahl, O. (2007). Cathepsin-cleaved Bid promotes apoptosis in human neutrophils via oxidative stress-induced lysosomal membrane permeabilization. *Journal of Leukocyte Biology*, *81*(5), 1213–1223. <http://doi.org/10.1189/jlb.0506359>
- Bolognese, A., Correale, G., Manfra, M., Lavecchia, A., Mazzoni, O., Novellino, E., ... Loddo, R. (2002). Antitumor agents. 1. Synthesis, biological evaluation, and molecular modeling of 5H-pyrido[3,2-a]phenoxazin-5-one, a compound with potent antiproliferative activity. *J Med Chem*, *45*, 5205–5216. <http://doi.org/jm020913z> [pii]
- Bolognese, A., Correale, G., Manfra, M., Lavecchia, A., Mazzoni, O., Novellino, E., ... Loddo, R. (2002). Antitumor agents. 2. Synthesis, structure - Activity relationships, and biological evaluation of substituted 5H-pyridophenoxazin-5-ones with potent antiproliferative activity. *Journal of Medicinal Chemistry*, *45*(24), 5217–5223. <http://doi.org/10.1021/jm020918w>
- Bolognese, A., Correale, G., Manfra, M., Lavecchia, A., Novellino, E., and Pepe, S. (2006). Antitumor Agents. 5. Synthesis, Structure–Activity Relationships, and Biological Evaluation of Dimethyl-5 H -pyridophenoxazin-5-ones, Tetrahydro-5 H -benzopyridophenoxazin-5-ones, and 5 H -Benzopyridophenoxazin-5-ones with Potent Antiproliferative Activit. *Journal of Medicinal Chemistry*, *49*(17), 5110–5118. <http://doi.org/10.1021/jm050745l>
- Boya, P., and Kroemer, G. (2008). Lysosomal membrane permeabilization in cell death. *Oncogene*, *27*(50), 6434–6451. <http://doi.org/10.1038/onc.2008.310>
- Boya, P., Reggiori, F., and Codogno, P. (2013). Emerging regulation and functions of autophagy. *Nature Cell Biology*, *15*(7), 713–720. <http://doi.org/10.1038/ncb2788>
- Braun, R. J., and Westermann, B. (2011). Mitochondrial dynamics in yeast cell death and aging.

Biochemical Society Transactions, 39(5), 1520–1526.
<http://doi.org/10.1042/BST0391520>

- Büttner, S., Eisenberg, T., Herker, E., Carmona-Gutierrez, D., Kroemer, G., and Madeo, F. (2006). Why yeast cells can undergo apoptosis: Death in times of peace, love, and war. *Journal of Cell Biology*, 175(4), 521–525. <http://doi.org/10.1083/jcb.200608098>
- Carmona-Gutierrez, D., Bauer, M. A., Zimmermann, A., Aguilera, A., Austriaco, N., Ayscough, K., ... Madeo, F. (2018). Guidelines and recommendations on yeast cell death nomenclature. *Microbial Cell*, 5(1), 4–31. <http://doi.org/10.15698/mic2018.01.607>
- Carmona-Gutierrez, D., Eisenberg, T., Büttner, S., Meisinger, C., Kroemer, G., and Madeo, F. (2010). Apoptosis in yeast: Triggers, pathways, subroutines. *Cell Death and Differentiation*, 17(5), 763–773. <http://doi.org/10.1038/cdd.2009.219>
- Chen, Y., and Klionsky, D. J. (2011). The regulation of autophagy - unanswered questions. *Journal of Cell Science*, 124(2), 161–170. <http://doi.org/10.1242/jcs.064576>
- Cheng, W.-C., Leach, K. M., and Hardwick, J. M. (2008). Mitochondrial death pathways in yeast and mammalian cells. *Biochimica et Biophysica Acta*, 1783(7), 1272–9. <http://doi.org/10.1016/j.bbamcr.2008.04.012>
- Chin, C., Donaghey, F., Helming, K., McCarthy, M., and Rogers, S. (2014). Deletion of AIF1 but not of YCA1 / MCA1 protects *Saccharomyces cerevisiae* and *Candida albicans* cells from caspofungin-induced programmed cell death, 1(2), 58–63.
- Chwieralski, C. E., Welte, T., and Bühling, F. (2006). Cathepsin-regulated apoptosis. *Apoptosis*, 11(2), 143–149. <http://doi.org/10.1007/s10495-006-3486-y>
- Clarke, P. G., and Clarke, S. (1996). Nineteenth century research on naturally occurring cell death and related phenomena. *Anat Embryol Dev*, 193, 81–99. <http://doi.org/10.1007/BF00214700>
- Duina, A. A., Miller, M. E., and Keeney, J. B. (2014). Budding yeast for budding geneticists: A primer on the *Saccharomyces cerevisiae* model system. *Genetics*, 197(1), 33–48. <http://doi.org/10.1534/genetics.114.163188>
- Eskelinen, E. L. (2006). Roles of LAMP-1 and LAMP-2 in lysosome biogenesis and autophagy. *Molecular Aspects of Medicine*, 27(5–6), 495–502. <http://doi.org/10.1016/j.mam.2006.08.005>
- Falcone, C., and Mazzoni, C. (2016). External and internal triggers of cell death in yeast. *Cellular and Molecular Life Sciences*, 73(11–12), 2237–2250. <http://doi.org/10.1007/s00018-016-2197-y>
- Fannjiang, Y., Cheng, W. C., Lee, S. J., Qi, B., Pevsner, J., McCaffery, J. M., ... Basañez, G. (2004). Mitochondrial fission proteins regulate programmed cell death in yeast. *Genes Dev*, 18, 2785–2797. <http://doi.org/10.1101/gad.1247904.istics>

- Farrugia, G., and Balzan, R. (2012). Oxidative Stress and Programmed Cell Death in Yeast. *Frontiers in Oncology*, 2(June), 1–21. <http://doi.org/10.3389/fonc.2012.00064>
- Fehrenbacher, N., Bastholm, L., Kirkegaard-Sørensen, T., Ram, B., Bøttzauw, T., Nielsen, C., ... Jäättelä, M. (2008). Sensitization to the lysosomal cell death pathway by oncogene-induced down-regulation of lysosome-associated membrane proteins 1 and 2. *Cancer Research*, 68(16), 6623–6633. <http://doi.org/10.1158/0008-5472.CAN-08-0463>
- Feng, Y., He, D., Yao, Z., and Klionsky, D. J. (2014). The machinery of macroautophagy. *Cell Research*, 24(1), 24–41. <http://doi.org/10.1038/cr.2013.168>
- Ferreira, J. (2017). *Characterization of vacuole permeabilization and HMGB1 nuclear release in the yeast cell death induced by a benzo[a]phenoxazine derivative. Master thesis.* Universidade do Minho.
- Frade, V. H. J., Gonçalves, M. S. T., and Moura, J. C. V. P. (2005). Synthesis and fluorescence properties of side-chain carboxylated 5,9-diaminobenzo[a]phenoxazinium salts. *Tetrahedron Letters*, 46(30), 4949–4952. <http://doi.org/10.1016/j.tetlet.2005.05.105>
- Frade, V. H. J., Sousa, M. J., Moura, J. C. V. P., and Gonçalves, M. S. T. (2007). Synthesis, characterisation and antimicrobial activity of new benzo[a]phenoxazine based fluorophores. *Tetrahedron Letters*, 48(47), 8347–8352. <http://doi.org/10.1016/j.tetlet.2007.09.108>
- Frade, V. H. J., Sousa, M. J., Moura, J. C. V. P., and Gonçalves, M. S. T. (2008). Synthesis of naphtho[2,3-a]phenoxazinium chlorides: Structure-activity relationships of these heterocycles and benzo[a]phenoxazinium chlorides as new antimicrobials. *Bioorganic and Medicinal Chemistry*, 16(6), 3274–3282. <http://doi.org/10.1016/j.bmc.2007.12.013>
- Fuchs, Y., and Steller, H. (2011). Programmed Cell Death in Animal Development and Disease. *Cell*, 147(4), 742–758. <http://doi.org/10.1016/j.cell.2011.10.033>
- Fuchs, Y., and Steller, H. (2015). Live to die another way: Modes of programmed cell death and the signals emanating from dying cells. *Nature Reviews Molecular Cell Biology*, 16(6), 329–344. <http://doi.org/10.1038/nrm3999>
- Galluzzi, L., Bravo-San Pedro, J. M., Vitale, I., Aaronson, S. A., Abrams, J. M., Adam, D., ... Kroemer, G. (2015). Essential versus accessory aspects of cell death: Recommendations of the NCCD 2015. *Cell Death and Differentiation*, 22(1), 58–73. <http://doi.org/10.1038/cdd.2014.137>
- Galluzzi, L., Vitale, I., Abrams, J. M., Alnemri, E. S., Baehrecke, E. H., Blagosklonny, M. V., ... Kroemer, G. (2012). Molecular definitions of cell death subroutines: Recommendations of the Nomenclature Committee on Cell Death 2012. *Cell Death and Differentiation*, 19(1), 107–120. <http://doi.org/10.1038/cdd.2011.96>
- Guicciardi, M. E., Leist, M., and Gores, G. J. (2004). Lysosomes in cell death. *Oncogene*, 23(16 REV. ISS. 2), 2881–2890. <http://doi.org/10.1038/sj.onc.1207512>

- Iwata, A., Yamaguchi, T., Sato, K., Yoshitake, N., and Tomoda, A. (2005). Suppression of proliferation of poliovirus and porcine parvovirus by novel phenoxazines, 2-amino-4,4 alpha-dihydro-4 alpha-7-dimethyl-3H-phenoxazine-3-one and 3-amino-1,4 alpha-dihydro-4 alpha-8-dimethyl-2H-phenoxazine-2-one. *Biological and Pharmaceutical Bulletin*, 28(5), 905–907. <http://doi.org/10.1248/bpb.28.905>
- Kim, I., Shu, C. W., Xu, W., Shiau, C. W., Grant, D., Vasile, S., ... Reed, J. C. (2009). Chemical biology investigation of cell death pathways activated by endoplasmic reticulum stress reveals cytoprotective modulators of ASK1. *Journal of Biological Chemistry*, 284(3), 1593–1603. <http://doi.org/10.1074/jbc.M807308200>
- Kirkegaard, T., and Jäättelä, M. (2009). Lysosomal involvement in cell death and cancer. *Biochimica et Biophysica Acta - Molecular Cell Research*, 1793(4), 746–754. <http://doi.org/10.1016/j.bbamcr.2008.09.008>
- Klionsky, D. J., Baehrecke, E. H., Brumell, J. H., Chu, C. T., Codogno, P., Cuervo, A. M., ... Tooze, S. A. (2011). A comprehensive glossary of autophagy-related molecules and processes (2nd edition). *Autophagy*, 7(11), 1273–1294. <http://doi.org/10.4161/auto.7.11.17661>
- Kroemer, G., Galluzzi, L., Vandenabeele, P., Abrams, J., Alnemri, E. S., Baehrecke, E. H., ... Melino, G. (2009). Classification of cell death: Recommendations of the Nomenclature Committee on Cell Death 2009. *Cell Death and Differentiation*, 16(1), 3–11. <http://doi.org/10.1038/cdd.2008.150>
- Kroemer, G., and Jäättelä, M. (2005). Lysosomes and autophagy in cell death control. *Nature Reviews Cancer*, 5(11), 886–897. <http://doi.org/10.1038/nrc1738>
- Kumar, N., and Sharma, A. (2006). Antimicrobial screening and synthesis of some novel benzo phenothiazines and ribofuranosides. *Indian Journal of ...*, 45(March), 747–751. Retrieved from <http://nopr.niscair.res.in/handle/123456789/6389>
- Kwolek-Mirek, M., and Zadrag-Tecza, R. (2014). Comparison of methods used for assessing the viability and vitality of yeast cells. *FEMS Yeast Research*, 14(7), 1068–1079. <http://doi.org/10.1111/1567-1364.12202>
- Leitão, M. I. P. S. (2015). *Síntese, atividade antifúngica e padrão de marcação em células de Saccharomyces cerevisiae de novos derivados fluorescentes de benzo[a]fenoxazina*. Universidade do Minho.
- Li, S. C., and Kane, P. M. (2009). The yeast lysosome-like vacuole: Endpoint and crossroads. *Biochimica et Biophysica Acta - Molecular Cell Research*, 1793(4), 650–663. <http://doi.org/10.1016/j.bbamcr.2008.08.003>
- Lockshin, R. A., and Williams, C. M. (1964). Programmed cell death-II. Endocrine potentiation of the breakdown of the intersegmental muscles of silkmoths. *Journal of Insect Physiology*, 10(4), 643–649. [http://doi.org/10.1016/0022-1910\(64\)90034-4](http://doi.org/10.1016/0022-1910(64)90034-4)
- Lopes, C. M. F. (2015). *Molecular pathways involved in the yeast cell death induced by a*

benzo[a]phenoxazine derivative. Universidade do Minho.

- Ludovico, P., Madeo, F., and Silva, M. T. (2005). Yeast programmed cell death: An intricate puzzle. *IUBMB Life*, *57*(3), 129–135. <http://doi.org/10.1080/15216540500090553>
- Luzio, J. P., Pryor, P. R., and Bright, N. A. (2007). Lysosomes: Fusion and function. *Nature Reviews Molecular Cell Biology*, *8*(8), 622–632. <http://doi.org/10.1038/nrm2217>
- Madeo, F., Fröhlich, E., and Fröhlich, K. U. (1997). A yeast mutant showing diagnostic markers of early and late apoptosis. *Journal of Cell Biology*, *139*(3), 729–734. <http://doi.org/10.1083/jcb.139.3.729>
- Marques, C., Oliveira, C. S. F., Alves, S., Chaves, S. R., Coutinho, O. P., Côrte-Real, M., and Preto, A. (2013). Acetate-induced apoptosis in colorectal carcinoma cells involves lysosomal membrane permeabilization and cathepsin D release. *Cell Death and Disease*, *4*(2), e507. <http://doi.org/10.1038/cddis.2013.29>
- Mason, D. A., Shulga, N., Undavai, S., Ferrando-May, E., Rexach, M. F., and Goldfarb, D. S. (2005). Increased nuclear envelope permeability and Pep4p-dependent degradation of nucleoporins during hydrogen peroxide-induced cell death. *FEMS Yeast Research*, *5*(12), 1237–1251. <http://doi.org/10.1016/j.femsyr.2005.07.008>
- Mazzoni, C., and Falcone, C. (2008). Caspase-dependent apoptosis in yeast. *Biochimica et Biophysica Acta - Molecular Cell Research*, *1783*(7), 1320–1327. <http://doi.org/10.1016/j.bbamcr.2008.02.015>
- Patil, V. S., Padalkar, V. S., Phatangare, K. R., Umape, P. G., Borase, B. N., and Sekar, N. (2015). Synthesis, Characterization, and Antibacterial Activity of Novel (1H-Benzo[d]imidazole-2-yl)-6-(diethylamino)-3H-one-xanthene, Phenoxazine, and Oxazine. *Journal of Heterocyclic Chemistry*, *52*(1), 124–129. <http://doi.org/10.1002/jhet.1998>
- Pereira, C., Camougrand, N., Manon, S., Sousa, M. J., and Côrte-Real, M. (2007). ADP/ATP carrier is required for mitochondrial outer membrane permeabilization and cytochrome c release in yeast apoptosis. *Molecular Microbiology*, *66*(3), 571–582. <http://doi.org/10.1111/j.1365-2958.2007.05926.x>
- Pereira, C., Chaves, S., Alves, S., Salin, B., Camougrand, N., Manon, S., ... Côrte-Real, M. (2010). Mitochondrial degradation in acetic acid-induced yeast apoptosis: The role of Pep4 and the ADP/ATP carrier. *Molecular Microbiology*, *76*(6), 1398–1410. <http://doi.org/10.1111/j.1365-2958.2010.07122.x>
- Pereira, C., Silva, R. D., Saraiva, L., Johansson, B., Sousa, M. J., and Côrte-Real, M. (2008). Mitochondria-dependent apoptosis in yeast. *Biochimica et Biophysica Acta - Molecular Cell Research*, *1783*(7), 1286–1302. <http://doi.org/10.1016/j.bbamcr.2008.03.010>
- Pereira, H., Oliveira, C. S. F., Castro, L., Preto, A., Chaves, S. R., and Corte-Real, M. (2015). Yeast as a tool to explore cathepsin D function. *Microbial Cell*, *2*(7), 225–234. <http://doi.org/10.15698/mic2015.07.212>

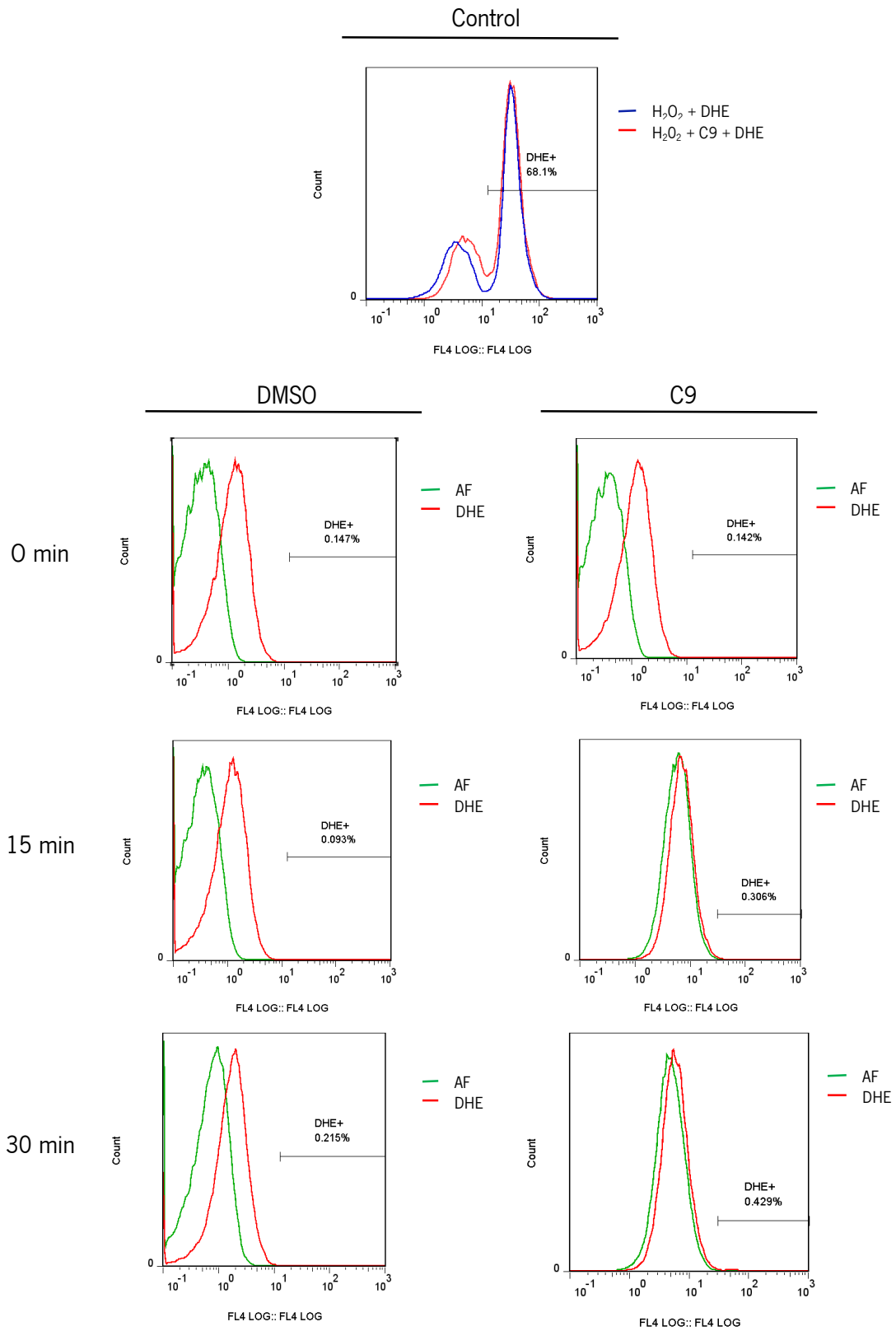
- Pereira, H. P. F. (2015). *The role of Pep4p , the vacuolar yeast protease ortholog of human cathepsin D , in mitochondria-dependent apoptosis*. Universidade do Minho.
- Pinton, P., Giorgi, C., Siviero, R., Zecchini, E., and Rizzuto, R. (2008). Calcium and apoptosis: ER-mitochondria Ca²⁺ transfer in the control of apoptosis. *Oncogene*, 27(50), 6407–6418. <http://doi.org/10.1038/onc.2008.308>
- Plesca, D., Mazumder, S., and Almasan, A. (2008). Chapter 6 DNA Damage Response and Apoptosis. *Methods in Enzymology*, 446(8), 107–122. [http://doi.org/10.1016/S0076-6879\(08\)01606-6](http://doi.org/10.1016/S0076-6879(08)01606-6)
- Postis, V., De Marcos Lousa, C., Arnou, B., Lauquin, G. J. M., and Trézéguet, V. (2005). Subunits of the yeast mitochondrial ADP/ATP carrier: Cooperation within the dimer. *Biochemistry*, 44(45), 14732–14740. <http://doi.org/10.1021/bi051648x>
- Ring, J., Sommer, C., Carmona-Gutierrez, D., Ruckenstuhl, C., Eisenberg, T., and Madeo, F. (2012). The metabolism beyond programmed cell death in yeast. *Experimental Cell Research*, 318(11), 1193–1200. <http://doi.org/10.1016/j.yexcr.2012.03.019>
- Rodrigues, J., Silva, R. D., Noronha, H., Pedras, A., Gerós, H., and Côrte-Real, M. (2013). Flow cytometry as a novel tool for structural and functional characterization of isolated yeast vacuoles. *Microbiology (United Kingdom)*, 159(PART 5), 848–856. <http://doi.org/10.1099/mic.0.062570-0>
- Scott, I., and Logan, D. C. (2008). Mitochondria and cell death pathways in plants. *Plant Signaling and Behavior*, 3(7), 475–477. <http://doi.org/10.1111/j.1469-8137.2007.02255.x>. www.landesbioscience.com
- Serrano-Puebla, A., and Boya, P. (2016). Lysosomal membrane permeabilization in cell death: new evidence and implications for health and disease. *Annals of the New York Academy of Sciences*, 1371(1), 30–44. <http://doi.org/10.1111/nyas.12966>
- Shimamoto, T., Tomoda, a, Ishida, R., and Ohyashiki, K. (2001). Antitumor effects of a novel phenoxazine derivative on human leukemia cell lines in vitro and in vivo. *Clinical Cancer Research : An Official Journal of the American Association for Cancer Research*, 7(3), 704–708.
- Silva, G. A., Costa, L. M. M., Brito, F. C. F., Miranda, A. L. P., Barreiro, E. J., and Fraga, C. A. M. (2004). New class of potent antinociceptive and antiplatelet 10H-phenothiazine-1-acylhydrazone derivatives. *Bioorganic and Medicinal Chemistry*, 12(12), 3149–3158. <http://doi.org/10.1016/j.bmc.2004.04.009>
- Simon, H. U., Haj-Yehia, A., and Levi-Schaffer, F. (2000). Role of reactive oxygen species (ROS) in apoptosis induction. *Apoptosis*, 5(5), 415–418. <http://doi.org/10.1023/A:1009616228304>
- Smith, M., and Wilkinson, S. (2017). ER homeostasis and autophagy. *Essays in Biochemistry*, 61(6), 625–635. <http://doi.org/10.1042/EBC20170092>

- Song, X., Kassaye, D. S., and Foley, J. W. (2008). 5,9-Diaminodibenzo[a,j]phenoxazinium chloride: A rediscovered efficient long wavelength fluorescent dye. *Journal of Fluorescence*, *18*(2), 513–518. <http://doi.org/10.1007/s10895-007-0293-y>
- Soto, C. Y., Andreu, N., Gibert, I., and Luquin, M. (2002). Simple and Rapid Differentiation of Mycobacterium tuberculosis H37Ra from M. tuberculosis Clinical Isolates through Two Cytochemical Tests Using Neutral Red and Nile Blue Stains Simple and Rapid Differentiation of Mycobacterium tuberculosis H37Ra from M. tuberculosis. *Society*, *40*(8), 3021–3024. <http://doi.org/10.1128/JCM.40.8.3021>
- Sousa, M. J., Azevedo, F., Pedras, A., Marques, C., Coutinho, O. P., Preto, A., ... Côrte-Real, M. (2011). Vacuole–mitochondrial cross-talk during apoptosis in yeast: a model for understanding lysosome–mitochondria-mediated apoptosis in mammals. *Biochemical Society Transactions*. <http://doi.org/10.1042/BST0391533>
- Sousa, M. J., Ludovico, P., Rodrigues, F., Leão, C., and Côrte-Real, M. (2012). Stress and Cell Death in Yeast Induced by Acetic Acid. In *Cell Metabolism - Cell Homeostasis and Stress Response* (Dr. Paula). InTech. <http://doi.org/10.5772/27726>
- Torggler, R., Papinski, D., and Kraft, C. (2017). Assays to Monitor Autophagy in Saccharomyces cerevisiae. *Cells*, *6*(3), 23. <http://doi.org/10.3390/cells6030023>
- Vakifahmetoglu-Norberg, H., Ouchida, A. T., and Norberg, E. (2017). The role of mitochondria in metabolism and cell death. *Biochemical and Biophysical Research Communications*, *482*(3), 426–431. <http://doi.org/10.1016/j.bbrc.2016.11.088>
- Wesolowska, O., Molnar, J., Westman, G., Samuelsson, K., Kawase, M., Ocsovszki, I., ... Michalak, K. (2006). Benzo[a]phenoxazines: A new group of potent P-glycoprotein inhibitors. *In Vivo*, *20*(1), 109–114.

Chapter VII

Supplementary data

VII. Supplementary data



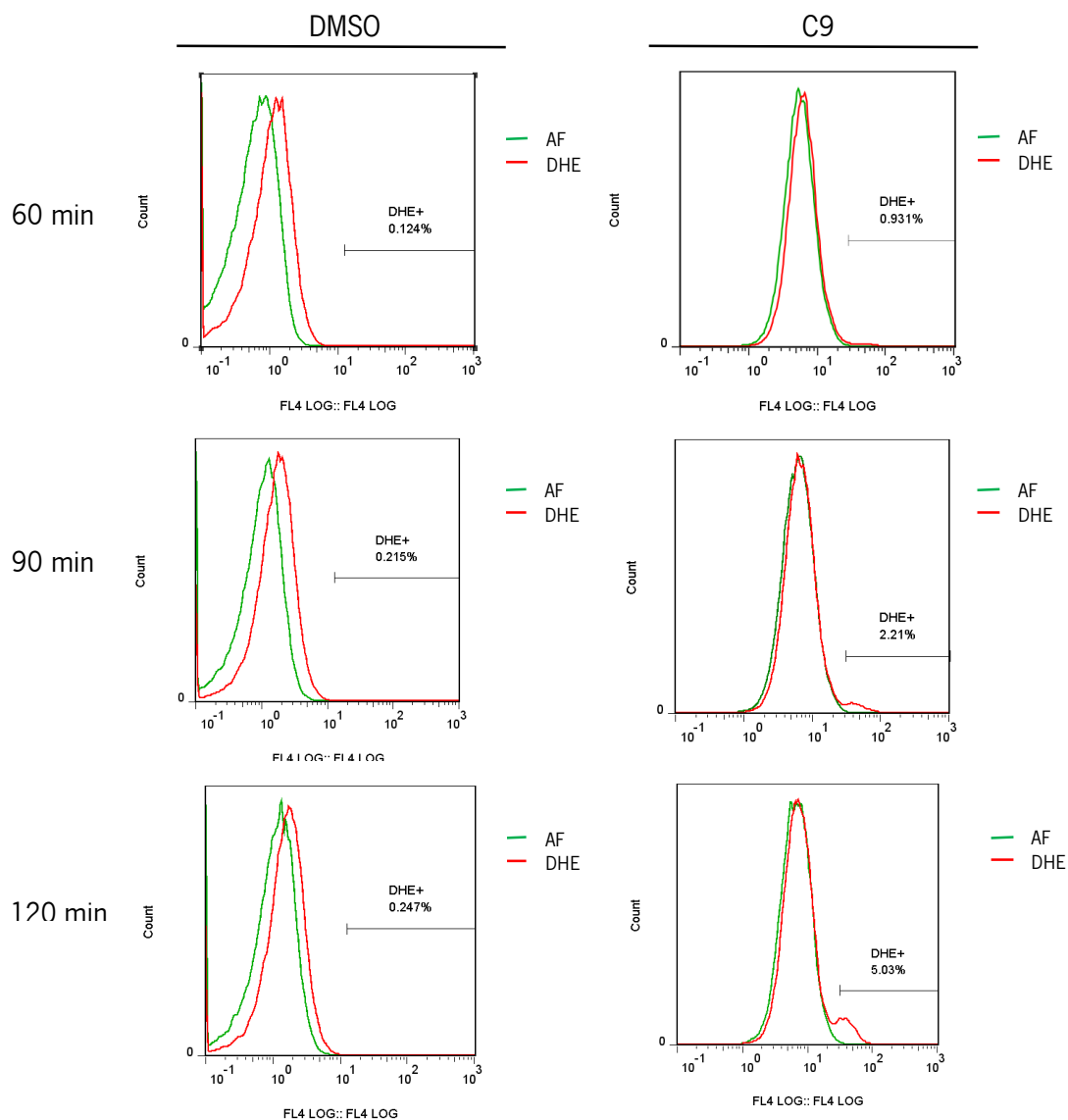
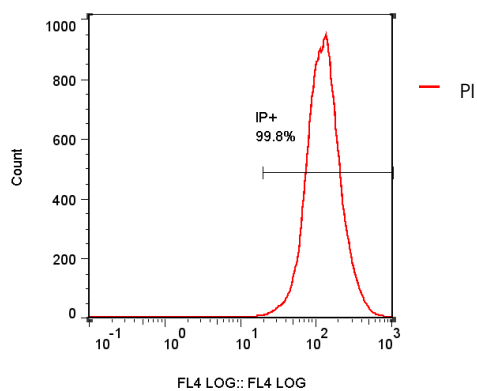


Figure VII.1 - Analysis of reactive oxygen species (ROS) accumulation in response to C9 treatment - Representative histograms of the effect of C9 and DMSO (negative control) on ROS accumulation of BY 4741 wild-type cells. Yeast cells were treated with C9 (7.5 μM) and DMSO (0.038%). As a positive control for DHE staining cells treated with hydrogen peroxide (H_2O_2) were used. For flow cytometry analysis, the cells were collected at different time points before (time 0) and after 15, 30, 60, 90 and 120 minutes of treatment and then stained with $2\mu\text{g ml}^{-1}$ of DHE. AF – Autofluorescence.

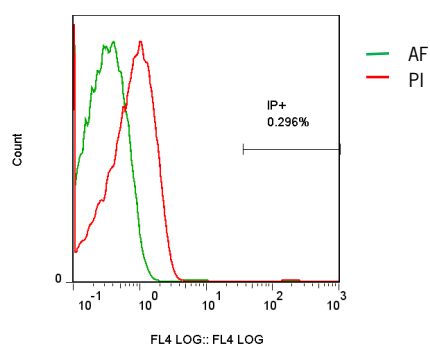
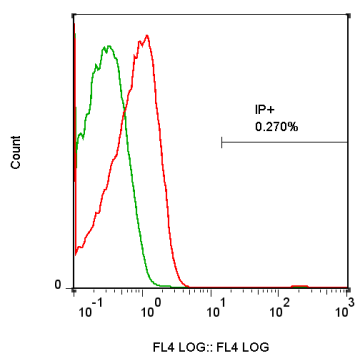
Control



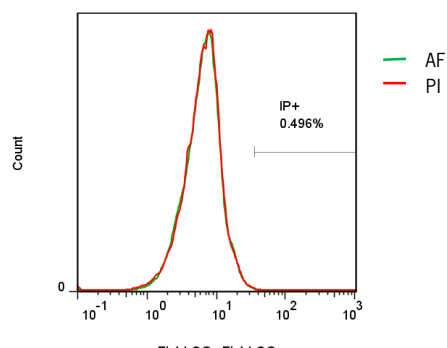
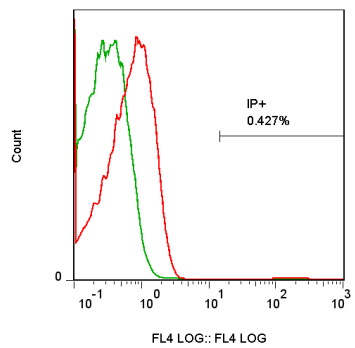
DMSO

C9

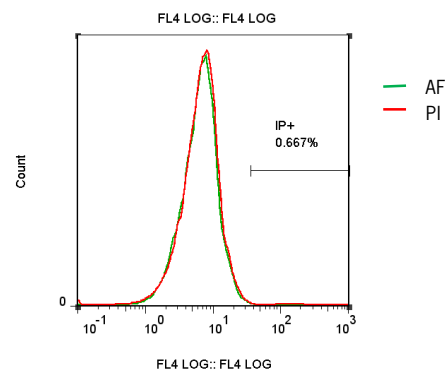
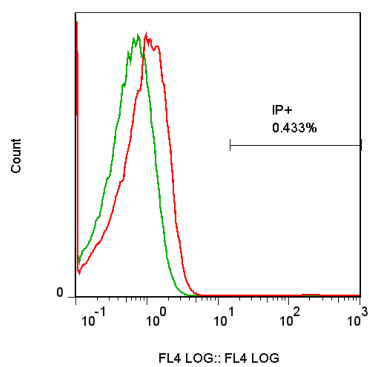
0 min



30 min



60 min



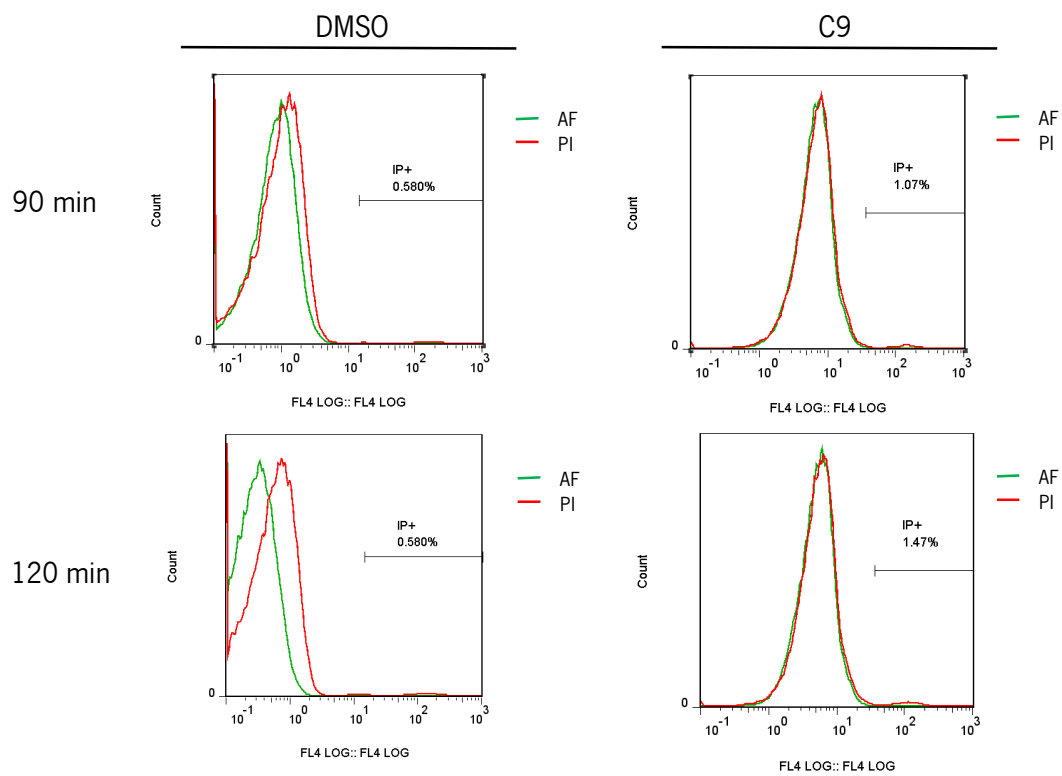


Figure VII.2 - Analysis of plasma membrane integrity in response to C9 – Representative histograms of the effect of C9 and DMSO (negative control) on plasma membrane integrity of BY 4741 wild-type cells stained with propidium iodide (PI). Yeast cells were treated with C9 (7.5 μM) and DMSO (0.038%). Boiled cells are used as a positive control for PI staining. For flow cytometry analysis the cells were collected at different time points before (time 0) and after 15, 30, 60, 90 and 120 minutes of treatment and then stained with $2\mu\text{g ml}^{-1}$ of PI. AF – Autofluorescence.